ENERGY INTERACTION OF VERTICAL AXIS WIND TURBINES WORKING IN PAIRS

A Thesis Submitted to
the Graduate School of Engineering and Science of
İzmir Institute of Technology
in Partial Fulfillment of the Requirements for the Degree of

MASTER OF SCIENCE

in Energy Engineering

by

Özgür GENCER

March 2023
İZMİR

ACKNOWLEDGMENTS

I would like to express my gratitude to my supervisor Assoc. Prof. Dr. Z. Haktan KARADENİZ for his guidance, criticism, and support throughout this thesis.

I would also like to extend my deepest gratitude to my family. Thank you for providing me with endless love, encouragement, and unwavering support throughout my academic journey. Your belief in me has been a constant source of motivation and inspiration

ABSTRACT

ENERGY INTERACTION OF VERTICAL AXIS WIND TURBINES WORKING IN PAIRS

The position of wind turbines relative to each other is important in terms of the performance of the turbines. The experiments and CFD studies in the literature have shown that Vertical Axis Wind Turbines (VAWTs) have a higher energy production per unit of land used than Horizontal Axis Wind Turbines (HAWTs) and it is found that there is a performance improvement of the VAWTs when they are operated in pairs.

In this thesis, CFD simulations of the H-type VAWTs working in pairs have been performed to investigate the energy interaction of the turbines. A standalone one-bladed VAWT was modelled based on the previous studies in the literature for the validation of the CFD methodology. Simulation parameters and simulation settings are compared with the reference study in the mesh independency analysis for four different mesh settings resulting in a deviation of up to %14, and in the time step sensitivity analysis for two different time steps corresponding to 0.25 and 0.5 degrees of azimuthal angle increments resulting in a deviation of up to %15. 1, 2, and 3 bladed stand-alone turbines are investigated to reveal the effect of the inter-turbine blade interaction on the energy output. A pair of co-rotating turbines configuration is analyzed at various Tip Speed Ratios (TSR) (1.7, 2.2, 3.3, 4.4) and at various distances between the turbines (3, 4, 6, 8, 10 diameters between axes) and compared with the standalone VAWT for each configuration.

The results of CFD simulations show that adding blades to the standalone VAWT results in a more stable moment coefficient, but it also leads to a decrease in the power coefficient at high TSRs. The co-located turbines cause flow disruption for the VAWTs working in pairs operating at unstable TSRs (<2), resulting in a performance reduction of up to 13.5%. Increasing the distance between turbines minimize the negative effect of disruption and improves turbine performance. As the TSR increases to a stable operation, the existence of the second turbine affects the energy output of both turbines positively, with the highest performance increase of 46% observed at TSR 3.3 when the turbines were placed closest to each other at 3D. The positive effect of the neighbouring turbine decreases as the distance between the turbines increase and the impact of distance between turbines on performance vanishes for the downstream turbine at 8D.

ÖZET

EŞLİ ÇALIŞAN DÜŞEY EKSENLİ RÜZGÂR TÜRBİNLERİNİN ENERJİ ETKİLEŞİMİ

Rüzgar türbinlerinin birbirlerine göre pozisyonu, türbin performansı açısından önemlidir. Literatürdeki deney ve hesaplamalı akışkanlar dinamiği simülasyon çalışmalarında; Düşey Eksenli Rüzgâr Türbinlerin (DERT), birim yerleşim alanı başına Yatay Eksenli Rüzgâr Türbinlerine (YERT) göre daha verimli olduğu görülmüş ve eş çalışan DERT'lerin performansında ciddi artış gözlemlenmiştir.

Bu tezde, H-tipi, eş çalışan, DERT'lerin hesaplamalı akışkanlar dinamiği simülasyonları yapılarak, türbinler arası enerji etkileşimi incelenmiştir. Yapılan akışkanlar dinamiği simülasyonlarını doğrulamak için tek kanatlı, tek çalışan DERT, literatürdeki çalışmalar referans alınarak modellenmiş ve farklı parametrelerde hesaplamalı akışkanlar dinamiği simülasyonları yapılmıştır. Ağdan bağımsızlık çalışmasında 4 farklı ağ yapısı kullanılarak, elde edilen sonuçlar referans çalışmayla karşılaştırılmış ve %14'e kadar sapma gözlenmiştir. Yapılan zamandan bağımsızlık çalışmasında ise 0.25 ve 0.5 derece dönüş açı artırımına karşılık gelen zaman adımları seçilerek, elde edilen sonuçlar karşılaştırılmış ve iki zaman adımı arasında %15'e kadar sapma gözlenmiştir. Tek, çift ve üç kanatlı; tek çalışan DERT'ler, türbin içindeki kanat etkileşiminin türbinin performansına olan etkisini incelemek için birbiriyle karşılaştırılmıştır. Eş çalışan DERT'lerin birbirine olan etkisini incelemek için türbinler arası mesafeler farklı uzunluklarda (3, 4, 6, 8, 10 türbin çapı, türbin merkezinden merkezine) ve farklı uç hız oranlarında (1.7, 2.2, 3.3 ve 4.4) seçilerek, elde edilen sonuçlar, tek çalışan DERT ile karşılaştırılmıştır.

Elde edilen sonuçlara göre; tek çalışan DERT'e eklenen her bir kanat, DERT'in daha stabil çalışmasını sağlarken, yüksek uç hız oranlarında çalışan DERT'in performansını düşürmüştür. Stabil olmayan uç hız oranlarında (<2), eş çalışan DERT'ler birbirinin akışını bozarak, tek çalışan DERT'e göre %12 daha az performans sergilemiştir. Türbinler arası mesafenin artmasıyla, türbinlerin birbirine olan etkisi azalmış ve türbinlerin performansı artmıştır. Eşli çalışan DERT'lerin maksimum performansı, %46 artışla 3.3 uç hız oranında, birbirine en yakın pozisyonda, türbinler arası 3 çap mesafede gözlenmiştir. 8 çap mesafeden sonra türbinler arası mesafenin türbinlerin performansına olan etkisi kaybolmuştur.

TABLE OF CONTENTS

LIST OF FIGURES vi

LIST OF TABLES viii

LIST OF SYMBOLS ix

CHAPTER 1. INTRODUCTION 1

1.1. Thesis Overview 3

1.2. Literature Review 3

CHAPTER 2. SIMULATION METHOD 10

2.1. Navier Stokes Equations 10

2.2. Reynolds Averaged Navier Stokes Equations (RANS) 11

2.3. Shear-Stress Transport (SST) k-ω Model 12

2.4. Fundamentals of Vertical Axis Wind Turbines 14

2.5. Simulation Settings 18

2.6. Geometric Properties of Simulation Domain 21

2.7. CFD Simulations 25

2.7.1. Mesh Independency Analysis 25

2.7.2. Time Step Sensivity Analysis 29

CHAPTER 3. RESULTS AND DISCUSSION 34

3.1. Standalone Vertical Axis Wind Turbine 34

3.2. Results of Vertical Axis Wind Turbines That Working in Pairs 43

CHAPTER 4. CONCLUSION 51

CHAPTER 5. REFERENCES 53

LIST OF FIGURES

Figure **Page**

Figure 1.1 An example of Vertical Axis Wind Turbine *(1)* 2

Figure 2.1 Isometric view of a typical VAWT.....14

Figure 2.2 Velocity and Force Vectors applied on VAWT *(2)* 15

Figure 2.3 Typical changes in the angle of attack at a variety of tip speed ratios *(4)* 16

Figure 2.4 The position of the airfoil in relation to the azimuth angle on a turbine 20

Figure 2.5 Schematic view of the simulation domain of the Vertical Axis Wind Turbine with 1-bladed turbine 21

Figure 2.6 Mesh details of simulation domain 22

Figure 2.7 4-different turbine models.....23

Figure 2.8 Mesh Details of Airfoil and Airfoil Zone 24

Figure 2.9 Mesh details of 3-different turbine models 24

Figure 2.10 Mesh structures of the tip of the NACA0018 airfoil 25

Figure 2.11 Mesh independency analysis at 1.7 TSR 26

Figure 2.12 Mesh independency analysis at 2.2 TSR 27

Figure 2.13 Mesh independency analysis at 3.3 TSR 27

Figure 2.14 Mesh independency analysis at 4.4 TSR 28

Figure 2.15 Error rates of mesh independency analysis.....28

Figure 2.16 Time step sensitivity analysis at 1.7 TSR 30

Figure 2.17 Time step sensitivity analysis at 2.2 TSR 31

Figure 2.18 Time step sensitivity analysis at 3.3 TSR 31

Figure 2.19 Time step sensitivity analysis at 4.4 TSR 32

Figure 2.20 Time step sensitivity analysis at various TSR 33

Figure 2.21 Comparison between CFD simulations and reference study for the 1-bladed turbine model: Cp vs. TSR.....33

Figure 3.1 Moment Coefficient graph for 1-bladed turbine at different TSR values of 1.7, 2.2, 3.3 and 4.4.....35

Figure 3.2 Moment Coefficient graph for 2-bladed turbine at different TSR values of 1.7, 2.2, 3.3 and 4.4 36

Figure 3.3 Moment Coefficient graph for 3-bladed turbine at different TSR values of 1.7, 2.2, 3.3 and 4.4 37

Figure **Page**

Figure 3.4 Comparison between CFD simulations and published studies for the 3 different turbine model: Cp vs. TSR 37
Figure 3.5 Moment Coefficient at 1.7 TSR 38
Figure 3.6 Velocity counters at $\theta = 160°$ for the 3 different VAWT models and their first blades operating at 1.7 TSR A) One-bladed VAWT B) Two-bladed VAWT C) Three-bladed VAWT 39
Figure 3.7 Moment Coefficient at 2.2 TSR 40
Figure 3.8 Moment Coefficient at 3.3 TSR 40
Figure 3.9 Moment Coefficient at 4.4 TSR 41
Figure 3.10 Velocity counters at $\theta = 160°$ for the 3 different VAWT models and their first blades operating at 3.3 TSR A) One-bladed VAWT B) Two-bladed VAWT C) Three-bladed VAWT 42
Figure 3.11 Schematic view of the standalone working VAWT and a pair of VAWTs that are positioned Δy apart from each other 43
Figure 3.12 Instantaneous one-blade Cp for the Vertical Axis Wind Turbines working in pairs, compared to the isolated turbine at TSR 1.7 44
Figure 3.13 Instantaneous one-blade Cp for the Vertical Axis Wind Turbines working in pairs, compared to the isolated turbine at TSR 2.2 45
Figure 3.14 Instantaneous one-blade Cp for the Vertical Axis Wind Turbines working in pairs, compared to the isolated turbine at TSR 3.3 46
Figure 3.15 Instantaneous one-blade Cp for the Vertical Axis Wind Turbines working in pairs, compared to the isolated turbine at TSR 4.4 46
Figure 3.16 Cp Vs TSR 47
Figure 3.17 Comparison of power coefficient vs TSR 48
Figure 3.18 Normalized power coefficient values of Turbine-1 (Left) and Turbine-2 (Right) at various TSR's 49
Figure 3.19 Comparison of normalized power coefficient vs TSR 50

LIST OF TABLES

Table **Page**

Table 2.1 The simulation parameters of the CFD simulations.....18

Table 2.2 Solution Settings of CFD simulation 19

Table 2. 3 Geometric properties of the simulation domain.....22

Table 2. 4 Time steps for time step sensitivity analysis.....30

Table 3.1 Tip Speed Ratio Table…….34

LIST OF SYMBOLS

ABBREVIATIONS

VAWT	Vertical Axis Wind Turbine
HAWT	Horizontal Axis Wind Turbine
TSR	Tip Speed Ratio
NACA	National Advisory Commitee for Aeronautics
CFD	Computational Fluid Dynamics
RANS	Reynolds Averaged Navier-Stokes
SST	Shear Stress Transport
PRESTO	Pressure Staggering Option

SYMBOLS

F_N	Normal force (N)
F_T	Tangential force (N)
Re	Reynolds number
p	Pressure (Pa)
ρ	Fluid density (kg/m^3)
ρ_a	Air density (kg/m^3)
∇	Del operator
Δ	Laplacian
η	Kinematic viscosity (Nms/kg)
k	Kinetic energy of the turbulent flow
ω	Specific dissipation rate
Γ_k	Diffusivity of kinetic energy of the turbulent flow
Γ_ω	Specific dissipation rate
σ_k, σ_ω	Turbulent Prandtl numbers
μ_t	Turbulent viscosity
G_k	Generation of the kinetic energy
G_ω	Generation of the specific dissipation rate

Y_k	Dissipation of the kinetic energy of the turbulent flow
Y_ω	Specific dissipation rate
D_ω	Cross-diffusion modification term
F_1	Blending function
N_b	Number of blades
c	Airfoil chord length (m)
D	Diameter of the VAWT (m)
H	Blade span (m)
V_0	Free stream velocity (m/s)
$\overrightarrow{V_\theta}$	Tangential velocity vector (m/s)
$\overrightarrow{V_R}$	Relative velocity vector (m/s)
α	Angle of attack
θ	Azimuthal angle
λ	TSR
ω_r, Ω	Angular velocity (rad/s)
R	VAWT radius (m)
σ	Solidity
C_{Drag}	Drag coefficient
C_{Lift}	Lift coefficient
A	Swept area by the turbine (m^2)
τ_t	Rotor torque (Nm)
F_{Drag}	Drag force (N)
F_{Lift}	Lift force (N)
C_t	Tangential force coefficients
C_n	Normal force coefficients
C_m	Moment coefficient
$C_{m,avg}$	Averaged moment coefficient
P_m	Mechanical power (Watt)
C_p	Power coefficient
$C_{p,avg}$	Averaged power coefficient

CHAPTER 1

INTRODUCTION

Without energy, today's society would not be able to function the way it does. While fossil fuels are starting to run out, the focus in the energy production sector has changed over the years away from fossil fuels and toward renewable energy sources. Energy production from renewable energy sources, such as solar power, hydropower, and wind energy, are all examples of sustainable energy methods. In 2019, 15% of the total electricity produced in European Union countries was generated by wind energy**.** This rate increased by 1% compared to the previous year due to new installations and investment in wind turbines.

Using of wind energy has been a long-standing goal for many centuries. One of the earliest forms of wind energy was the vertical axis windmill, which was first developed by the Persians in the 10th century AD (*27*). These windmills were used to automate tasks such as grain grinding and irrigation. This design has been used for centuries and has significantly impacted how wind energy has been utilized over time.

In the early 20th century, Vertical Axis Wind Turbine (VAWT) designs were based on the idea of aerodynamic drag rather than aerodynamic lift. The turbine exposed to wind generates torque as wind pushes against blades. The use of aerodynamic lift, created by the difference in pressure due to the shape of the blade, is much more efficient than using drag. The first lift-based (VAWT) was invented by Georges Darrieus in France during the 1920s, who was granted a US patent in 1931 (*23*). VAWTs were widely used to power rural homes and small farms in the United States and Europe in the early 20th century. However, the widespread use of more efficient Horizontal Axis Wind Turbines (HAWTs) in the mid-twentieth century resulted in a decrease in the use of VAWTs. Over time, there was a shift in focus towards the HAWT, which was considered to be more efficient than the VAWT. The vast majority of efforts, investments, and research are focused on this particular wind turbine model. As a result, HAWTs are responsible for producing a significant portion of the electricity generated by wind energy.

Figure 1.1 An example of Vertical Axis Wind Turbine (*1*)

In addition, there is a growing interest in applying VAWT (Figure 1.1) for decentralized energy production in urban areas. The small VAWT is the most promising solution for urban and off-grid environments. Despite having a lower peak performance, they have become a valuable alternative to conventional turbines in urban applications because of specific features such as omnidirectional capabilities, lower noise emissions, and a nice appearance (*28*).

In addition to these features, VAWTs are simpler than HAWTs; for instance, the gearboxes of VAWTs can be briefly installed on the ground. This makes the process of installation and maintenance significantly less complicated and cheaper. Most importantly, they can be installed in a group and positioned closer together in an area. This arrangement allows for a positive interaction between the turbines, which can improve their overall performance and increase their output efficiency.

The primary aim of this thesis is to investigate the energy interactions VAWTs when operating in pairs. To ensure the accuracy of the CFD simulations, a 2-dimensional VAWT model was validated against a reference study from the literature. Subsequently, standalone working VAWTs with varying numbers of rotor blades were simulated at various TSR to explore the aerodynamic interactions between the blades in a systematic manner. The results of these CFD simulations were then compared with the results of the CFD simulations of co-located, co-rotating VAWTs placed at different inter-turbine distances, operated at various TSRs to comprehensively invastigate the aerodynamic influences like wake flow and flow disruption of the turbines on each other and its impact on their overall performance.

1.1. Thesis Overview

In the Introduction chapter, a brief summary of VAWT was presented, followed by a comprehensive review of the literature. This helped to highlight the importance of the subject and identify the limitations and drawbacks of the previous studies in the field.

In Chapter 2, the equations for the forces acting on the VAWT blades, Navier Stokes, Reynolds Averaged Navier Stokes equations, and the turbulence model used in the CFD simulations are presented. This chapter also covered the settings and parameters for the CFD simulations, as well as the geometric properties of the VAWT models. To demonstrate the accuracy of the CFD settings, a reference study was used for validation, and the chapter concluded with time-step sensitivity analysis and mesh independence analysis.

In the first part of Chapter 3, CFD simulations have been made for three different standalone VAWT models which are operating at various TSRs to investigate the aerodynamic impact of blades on each other and how it affects VAWT performance. In the second part, CFD simulations of the co-located and co-rotating VAWTs placed at various distances from each other have been made to investigate their energy interaction and its effect on the overall performance.

And finally, Chapter 4 offers a conclusion and insightful commentary.

1.2. Literature Review

The study of Stickland et al. (*6*) is one of the oldest studies on the H-type Darrieus VAWT. Computer codes for both two-and three-dimensional turbines were written. These codes were tested in a few scenarios in order to compare them with the usable experimental data. Furthermore, current vortex models are compared with simple momentum models.

In general, the study found that the vortex models and the basic momentum models have similar fits with respect to turbine performance. The turbine power coefficient appears to be accurately predicted by the vortex model for both two-dimensional rotors and three-dimensional rotors. On the normal force (F_N), the results of the study have been shown that the numerical study and the experimental study perfectly match.

Due to the results' similarity, the vortex models should be able to accurately estimate the major aerodynamic force component related to the rotor's structural integrity. However, in this study, the tangential force obtained from the numerical study and

the obtained from the experiment was not sufficiently fit each other. As a result, Strickland et. al suggested that a more improved experiment setup will accurately verify the tangential force (F_T).

In a previous study, simple vortex codes were compared to data obtained from an experiment rig that placed the VAWT in a tank full of water. These values were insufficient to verify Tangential Force (F_T). Hence, Vittecoq et al. (*7*) improved the experimental rig and the technic of the experiment to verify the tangential force (F_T). They changed the experiment method and used the air as a fluid instead of water. Despite using air instead of water as a fluid in the experiment, the normal force (F_N) obtained was identical to the ones obtained by Stricklands et al. (*6*). The tangential force follows the same pattern and has the same magnitude. The higher frequency content of the F_T curves differs. At last, the author indicates that dynamic stalling occurs at less than TSR 3.5.

The study of Kooiman et al. (*8*) focused on the effect of unsteady wind on VAWT's aerodynamic performance. An experimental test rig was built to investigate this subject. In this experimental setup, VAWT with 3-blades with NACA0015 profile, 2.5 meters in diameter and 3 meters in length were used. According to published experimental results, when the fluctuation of wind speed I_v is less than 0.15, it has been observed that the performance of VAWT decreases marginally. However, when the fluctuation of wind speed I_v exceeds 0.15, the performance of the VAWT is reduced by 3.6%. These results proved that VAWT could also be used in real-world conditions with a slight decrease in its performance.

When transitioning from laminar to turbulent flow, the VAWT's performance decreases significantly. Thus, the study of Castelli et al. (*9*) focused on this topic and compared the previously published experimental results (*10*) with the results of CFD simulations. In this published article, the same 2-dimensional VAWT with NACA0012 profile blade was simulated using commercial CFD on three different sub-grids. And it has been discovered that an accurate mesh setup on the airfoil boundary layer is required to calculate the laminar-to-turbulent transition accurately.

In terms of spatial and temporal discretization, Balduzzi et al. (*11*) believe that the CFD simulations with VAWT have not truly converged. For this reason, the focus has been placed on the required mesh and time step size to obtain accurate CFD results for VAWTs operating at various TSRs. With this purpose, the effect of various parameters, including tip speed ratio, mesh number and mesh size, azimuthal angle, and time step size on the results of CFD simulations of VAWT was studied. The 2-dimensional VAWT

with a single blade NACA0018 was used for CFD simulation in this study, which I also use as a reference in my thesis. According to the obtained results, the maximum torque was generated at TSR 3.3. In addition, Balduzzi et al. (*11*) stated that the difference between VAWT's stable operating speeds (TSR>3) and unstable operating speeds is due to the vortex that develops on the boundary layer of the airfoil when the VAWT is operating at an unstable speed. On TSR>3, it was observed that the obtained moment coefficient graph was smoother due to the absence of this vortex at the airfoil boundary layer.

The study of Rezaeiha et al. (*12*) investigates the effect of domain size and azimuthal angle increment on the efficiency of a 2-bladed VAWT that performs at TSR 4.5. They used the 2-dimensional CFD simulations with unsteady Reynolds-averaged Navier-Stokes (URANS) technique. According to the results of Rezaeiha et al. (*12*) CFD simulations, the turbines should be rotated at least 20 times and placed at least 10D away from the inlet and outlet of the fluid domain. In addition, they discovered that the width of the fluid domain should be at least 20D in order to minimize the effect of wind blockage, the rotor zone should be at least 1.5D, and the minimum azimuthal increment should be at least 0.5 degrees in order to minimize the effect of the temporal resolution. Although the study recommended that turbines be rotated for at least 20 turns during CFD simulations, the power coefficient value difference between 10 and 20 revolutions was just 5% on average. Hence, it may not be essential to continue the simulations for 20 turns, as the additional processing time may not be worth the marginal improvement in precision.

The experiment of Dabiri et al. (*13*) focused on how the arrangement of VAWTs affects their performance when used together in an array. They used a potential flow model to simulate VAWTs in different spatial configurations and compared the average power coefficient of a standalone working turbine to the expected average power coefficient of turbines in an array. They found that arranging the VAWTs in a pattern inspired by the vortices created by schooling fish, with sequential turbines rotating in opposite directions significantly improved the array performance coefficient. In fact, the power output of an array of 16x16 VAWTs using this configuration was found to be over 10 times greater than that of an array of HAWTs with the same land area. Dabiri et al. (*13*) also claimed that vortex interaction, rather than blocking effects from near wind turbines, is the dominant cause for the stream-tube contraction, which explains the increase in overall array performance.

In the study of Schatzle et al.'s (*14*) 2 bladed, 2 VAWTs were used and positioned 1.5D apart. They were tested in eight different configurations. The turbines were operated at TSR 3 during the experiment, as it was identified as the optimal point for maximum power output. The study utilized a vortex/lifting model to calculate the power output. The impact of free-stream turbulence was disregarded in the calculation. Schatzle et al. (*14*) found a significant power reduction in turbines aligned parallel to the fluid flow. Additionally, an increase in the tip-speed ratio for a fixed separation distance was found to boost the power output.

Dabiri et al. (*15*) conducted a well-known experiment that compared the power output per unit land area of VAWTs working in pairs with HAWTs. The experiment used 10-meter long, 1.2-meter diameter VAWTs located in various positions with counter-rotating adjustment. The results showed that the third VAWT, located in the downwind region of the two paired working VAWTs, experienced a significant decrease in performance due to wind blockage, especially at higher tip speed ratios. However, when the third VAWT was located at a distance of 4D, its performance increased by 5% compared to a standalone VAWT. The study found that paired VAWTs produced 18 W/m^2 of power output per unit land area and stated that this output could be increased up to 30 W/m^2 through a reconfiguration of the VAWTs. These results suggest that improving the arrangement of wind turbines can be just as effective as improving the design of the turbines in increasing the total energy output.

The experiment of Brownstein et al. (*16*) focused on how VAWTs affect each other's performance. In their experiments, they varied three parameters; the freestream wind direction, the distance between the turbines, and the relative rotational orientation of the turbines at a Reynolds value of $Re_D = 7.3 \text{ x } 10^4$. The test rig measurements used by Brownstein were 2.06 m wide, 1.97 m high, and 4.88 m long, and they used two industrial, five-bladed VAWTs in the experiment. The results were analyzed in three different regimes. The second turbine, located at a $\varphi°$ between the freestream and the downstream area, showed a significant reduction in performance when φ was between -40° and 30°. Both turbines showed an improvement in performance when φ was greater than 30° degrees. Performance reduced again when φ was below -40°, but the drop was less significant in co-rotating settings. Additionally, the effect of turbine spacing on performance was measured at distances of 1.25D, 1.5D, 2D, and 3D. The results showed that the distance between the turbines was significant, with turbine performance being inversely proportional to distance.

The experiment of Kinzel et al. (*17*) investigated the energy interaction between turbines by examining average and turbulent kinetic energy fluxes at a power plant site using 9 pairs of counter-rotating VAWTs. The turbines used in the study had a height of 6.1 meters and a diameter of 1.2 meters. Measurements were taken with a moving meteorology station between the turbine pairs, and it was found that the distance required for the wind velocity in the downwind area to reach 95% of the freestream velocity is 6D. This distance was half of what is required for modern HAWTs, but higher than the 4D, Dabiri et al.'s (*15*) experiment results. However, the study's point and asynchronous measurements were not sufficient for a detailed analysis of the energy transfer mechanisms between turbines. Therefore, the study provided a general evaluation and emphasized that the distance between turbines and properties such as TSR, solidity, and moment coefficient should be examined for a more thorough analysis.

The study of Zanforlin et al. (*18*) investigated how pairs of two different configurations of counter-rotating VAWTs interact and affect each other's performance. The study used CFD simulations to analyze the effects of various distances, freestream angles, and tip speed ratios on the performance of the VAWTs. Two different configurations were tested, and the results were compared to those of a standalone working VAWT. CFD simulations were conducted for VAWTs that were located 1.5D at each other's, rotating in clockwise and counterclockwise directions at 2.3 TSR and 3.2 TSR. The study found that the counterclockwise rotating turbine's performance improved by around 13% compared to a standalone working turbine. The physical mechanism behind the improvement in the performance was the increase in lateral velocities in front of the turbines and the use of higher momentum by the turbines due to the width of the low-velocity area in the downwind region. The study also examined the effect of airflow direction and found that the performance improvement occurred in the region of ±45 ° at the front and rear. Changing the distance between the turbines had a similar effect on performance. These results could be helpful in designing and optimizing wind turbine farms. Furthermore, the results obtained in the present study will be compared in detail with the CFD simulation results conducted by Zanforlin et al. (*18*) in Chapter 3.

In the study of Brusca et al. (*19*), 3-bladed VAWTs with Naca0018 profile were tested in the CFD simulations. The upstream turbine always rotated counterclockwise, while the second turbine placed downstream rotated in both clockwise and counterclockwise directions depending on the φ angle. The simulation results showed that turbine pairs had improvement in performance in all conditions where the φ was

greater than 0°, with the maximum performance achieved between φ 45° and 90°. The second turbine reached maximum power at an φ of +30° in the counter-rotating configuration, while performance continued to improve with increasing the φ angle in the co-rotating configuration. The first turbine reached maximum power at φ of 90° in both counter-rotating and co-rotating configurations. Overall, the simulation of 25 different layouts showed that turbine pairs improved each other's performance by 15%, with the optimal configuration being φ is 60° and the distance between turbines is 3D.

The study of Guilbot et al. (*20*) used CFD simulations to investigate the performance of a VAWT that is placed side-by-side and perpendicular to the freestream, with the Naca0018 profile, in pairs. The study aimed to determine how the distance between turbines and their rotational directions would affect their performance. The configurations were co-rotating and counter-rotating, with turbines placed at distances of 1.05D and 1.5D. The results showed that the VAWT working in pairs produced more power than standalone VAWTs. The normalized performance of VAWTs in pairs with 1.5D distance improved by 4%, and VAWTs in pairs with 3D distance improved by 7% in performance. However, in the configuration where the first turbine rotated clockwise and the second turbine rotated anti-clockwise, the turbines located at 1.05D distance achieved 4.5% more performance than the standalone working turbines, and the turbines located at 1.5D distance had 2.6% more performance than the standalone working turbines, regardless of the distance.

The study of De Tavernier et al. (*21*) utilized CFD simulations to evaluate the effects of various tip-speed ratios, distances, and rotation configurations on the performance of a 2-dimensional VAWT featuring 2 blades with NACA0015 profiles. The results indicate that the performance of turbines working in pairs is superior to standalone turbines. Specifically, the counter-up rotation configuration shows the highest performance gain, which is consistent with prior research by Guilbot et al. (*20*). Furthermore, the positive effect of this configuration on turbine performance was found to persist across varying inter-turbine distances. Notably, a performance increase was also observed with co-rotating turbines, although this effect occurred at a certain distance between the turbines. The study concludes that the use of turbine pairs can achieve a 10% performance improvement in power coefficient.

Based on a comprehensive review of existing literature, it was observed that in most studies and CFD simulations, the distance between turbines was often set at a narrow range, resulting in limited information on the effect of inter-turbine distance on turbine

performance. Additionally, the range of tip-speed ratios used in CFD simulations was set from a small range of area or kept constant, which makes it difficult to determine the impact of TSR on performance completely. Besides, in many studies, turbines were generally configured to be counter-rotating, thereby limiting the scope of the analyses. To address these limitations, this thesis aimed to investigate the impact of inter-turbine distance on the performance of vertical-axis wind turbines working in pairs under various TSRs. By selecting different inter-turbine distances, the study aimed to demonstrate the effect of distance on performance more clearly, alongside various TSRs. Furthermore, by choosing co-rotating turbine configurations, the study followed a different path from the existing literature in CFD simulations. The findings of this study are expected to provide additional information on the performance of VAWTs operating in pairs under specific TSRs and inter-turbine distances. By addressing the limitations of previous studies, this study could potentially contribute to the development of more efficient and cost-effective VAWT systems.

CHAPTER 2

SIMULATION METHOD

This chapter will provide details on the methods used in CFD simulations of VAWT. It will start by discussing the mathematical analysis methods for turbulence, including Navier-Stokes Equations, Reynolds-Averaged Navier-Stokes, and turbulence models derived from these equations which are all used in the CFD simulations in this thesis. Next, the equations for the forces acting on the VAWT will be given, to aid in understanding how the aerodynamic model of VAWT is developed.

2.1. Navier Stokes Equations

The Navier-Stokes equations are differential equations that can be used to mathematically model the behavior of any Newtonian fluid in any flow regime (*26*) but they will specifically be discussed in the context of turbulence.

Turbulence is a type of fluid motion that displays disorderly and unpredictable fluctuations in velocity, pressure, and other flow properties. It is a three-dimensional and time-varying phenomenon that arises when a fluid experiences significant disturbances, such as shear or instability, resulting in a highly disorganized and irregular flow pattern. However, despite the chaotic nature of turbulence, it can still be described mathematically using the Navier-Stokes equations, which are a set of partial differential equations that govern the behavior of fluid flows. Navier-Stokes equations are (*24*);

$$\frac{\partial \boldsymbol{\rho}}{\partial t} + \nabla \cdot (\rho \boldsymbol{u}) = 0 \tag{2.1}$$

$$\frac{\partial \boldsymbol{u}}{\partial t} + \boldsymbol{u} \cdot \nabla \boldsymbol{u} = -\frac{1}{\rho} \nabla p + \eta \Delta \boldsymbol{u} + \boldsymbol{g} \tag{2.2}$$

Equation 2.1 and Equation 2.2 are continity and momentum equations. Where ∇ is the del operator, Δ is the Laplacian, η is the kinematic viscosity and ρ is the fluid density. Since, the flow is incompressible, it is assumed constant. **u** is the velocity vector

which is function of space and time, and it can repsented with **u**(**x**,t). Similarly, **p**(**x**,t) is the pressure, ***g***(**x**,t) is the body force term.

As stated previously the Navier-Stokes equations are capable of modeling all types of fluid flow with highly turbulent flows but it requires a significant amount of computational resources and effort. Therefore, in order to obtain useful information, it is necessary to rely on the analysis of averaged quantities. The use of Reynolds decomposition on the Navier-Stokes equations can separate the turbulent fluctuations from the time-averaged flow, simplifying the equations and enabling the focus on the essential aspects of the flow. The Reynolds-Averaged Navier-Stokes (RANS) equations (*25*), which describe the mean flow, result from this simplification process and provide insights into the flow's significant features.

2.2. Reynolds Averaged Navier Stokes Equations (RANS)

The transport of the averaged flow quantities is governed by RANS equations, which simulate the full spectrum of turbulence patterns. Due to the significant reduction in computing effort and resources, the RANS-based modelling approach has found widespread adoption for real-world engineering purposes. The time-averaging formula of a function ($f(x_i, t)$) is;

$$\bar{f} = \lim_{T\to\infty} \frac{1}{T} \int_o^T f(x_i, t) dt \tag{2.3}$$

Reynolds averaging decomposes the solution variables of the instantaneous (exact) Navier-Stokes equations into the mean (time-averaged) and fluctuating components *(4)*. Considering pressure (p_i) and velocity (u_i);

$$\boldsymbol{p}_i = \bar{p}_i + p'_i \tag{2.4}$$

$$\boldsymbol{u}_i = \bar{u}_i + u'_i \tag{2.5}$$

where $\bar{p}_i$ and $\bar{u}_i$ are the mean, and p'_i and u'_i are the fluctuating components of the pressure and velocity, respectively. Reynolds-averaged Navier-Stokes (RANS) equations

are defined as Equations 2.6 and 2.7 They have the same structure as the Navier-Stokes equations, but the velocities and other variables in the solutions now represent averages over time as;

$$\frac{\partial \rho}{\partial t} + \frac{\partial(\rho \bar{u}_i)}{\partial x_i} = 0 \tag{2.6}$$

$$\frac{\partial}{\partial t}(\rho \bar{u}_i) + \frac{\partial}{\partial x_j}(\rho \bar{u}_i \bar{u}_j) = -\frac{\partial(\bar{p})}{\partial x_i} + \frac{\partial}{\partial x_j}\left[\mu\left(\frac{\partial u_i}{\partial x_j} + \frac{\partial u_j}{\partial x_i} - \frac{2}{3}\delta_{ij}\frac{\partial \bar{u}_m}{\partial x_m}\right)\right] + \frac{\partial}{\partial x_j}\left(-\rho\overline{u'_\iota u'_\jmath}\right) \tag{2.7}$$

$$\tau_{ij} = \mu\left(\frac{\partial u_i}{\partial x_j} + \frac{\partial u_j}{\partial x_i}\right) \tag{2.8}$$

where $\rho\overline{u'_\iota u'_\jmath}$ is a Reynolds stress tensor, R_{ij}.

2.3. Shear-Stress Transport (SST) k-ω Model

When trying to get realistic simulation results, selecting the appropriate turbulence model is absolutely necessary. Transition, separation, and reattachment of the flow to the airfoil surface are all important variables in VAWT analysis. In addition, since there is no turbulence model that fits every occasion, it is essential to choose the turbulence model that is most suited to these considerations. For this reason, simulations performed with the SST *k-ω* turbulence model, which is the in-built and pre-defined turbulence model in ANSYS Fluent.

As mentioned above, one of the popular 2 equation turbulence models, the Shear-Stress Transport (SST) k-ω, was used in this study for all the CFD simulations since it's more accurate and more reliable than the standard *k*-ω turbulence model *(5). E*quations 2.9 and 2.10 are the transport equations for the SST k-*ω* turbulence model. The k denotes the kinetic energy of the turbulent flow and the *ω* stands for the specific dissipation rate (*25*).

$$\frac{\partial}{\partial t}(\rho k) + \frac{\partial}{\partial x_i}(\rho k u_i) = \frac{\partial}{\partial x_j}\left(\Gamma_k \frac{\partial k}{\partial x_j}\right) + \widetilde{G_k} - Y_k + S_k \tag{2.9}$$

$$\frac{\partial}{\partial t}(\rho\omega) + \frac{\partial}{\partial x_i}(\rho\omega u_i) = \frac{\partial}{\partial x_j}\left(\Gamma_\omega \frac{\partial \omega}{\partial x_j}\right) + G_\omega - Y_\omega + D_\omega + S_\omega \tag{2.10}$$

Γ_k and Γ_ω are the effective diffusivity of kinetic energy of the turbulent flow and the specific dissipation rate. The equations of the effective diffusivities shown in 2.11 and 2.12.

$$\Gamma_k = \mu + \frac{\mu_t}{\sigma_k} \tag{2.11}$$

$$\Gamma_\omega = \mu + \frac{\mu_t}{\sigma_\omega} \tag{2.12}$$

Where σ_k and σ_ω are the turbulent Prandtl numbers and μ_t is the turbulent viscosity given below,

$$\mu_t = \frac{\rho k}{\omega} \tag{2.13}$$

G_k represents the generation of the kinetic energy of the turbulent flow, and G_ω represents the generation of the specific dissipation rate, where α is a constant.

$$G_k = -\rho\overline{u'_i u'_j}\left(\frac{\partial u_j}{\partial x_i}\right) \tag{2.14}$$

$$G_\omega = \alpha \frac{\omega}{k} G_k \tag{2.15}$$

Dissipation of the kinetic energy of the turbulent flow and specific dissipation rate represented by Y_k and Y_ω.

$$Y_k = \rho\beta^* k\omega \tag{2.16}$$

$$Y_\omega = \rho\beta\omega^2 \tag{2.17}$$

The D_ω in equation 2.18 represents the cross-diffusion modification term. F_1 is a blending function.

$$D_\omega = 2(1 - F_1)\rho\sigma_{\omega,2}\frac{1}{\omega}\frac{\partial k}{\partial x_j}\frac{\partial \omega}{\partial x_j} \tag{2.18}$$

2.4. Fundamentals of Vertical Axis Wind Turbines

Before moving on to the CFD modelling and its methods, a detailed summary of the underlying physics of general aerodynamics for VAWT will be explained to gain a better understanding of its working principle. Figure 2.1 displays an isometric view of a VAWT rotor, which includes two straight blades with an airfoil shape and large span to chord ratio. The blades are connected to the rotor's rotating shaft via struts, which provide structural support during rotation.

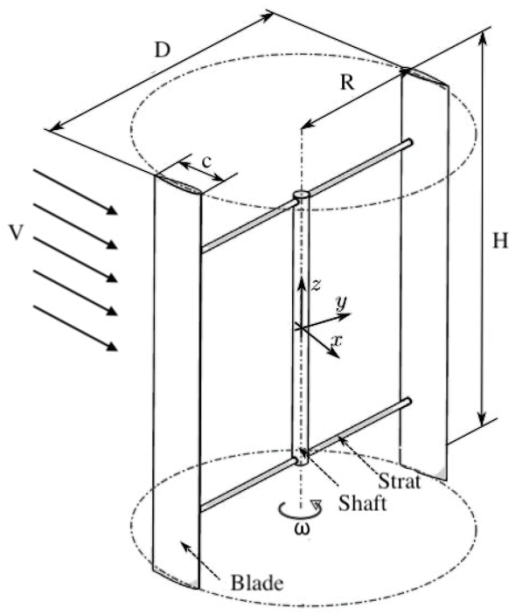

Figure 2.1 Isometric view of a typical VAWT

The number of blades is represented by N_b, the airfoil chord length is represented by c. D is the diameter of the VAWT turbine and H is the blade span. The VAWT performance can be predicted based on the aerodynamic force acting on each airfoil once the TSR and solidity are defined.

Figure 2.2 shows the velocity vectors and the force vectors on the VAWT. The free stream velocity is V_0 (m/s), $\overrightarrow{V_\theta}$ is the tangential velocity vector of the turbine. $\overrightarrow{V_R}$ is the relative velocity vector. Typically, the angle of attack (α), is defined as the angle between the direction of the relative velocity $(\overrightarrow{V_R})$ and the chord line of the blade.

$$\overrightarrow{V_\theta} + V_0 = \overrightarrow{V_R} \tag{2.19}$$

$$V_\theta = \omega_r R \tag{2.20}$$

$$V_R = \sqrt{(V_0 + V_\theta cos\theta)^2 + (V_\theta cos\theta)^2} \tag{2.21}$$

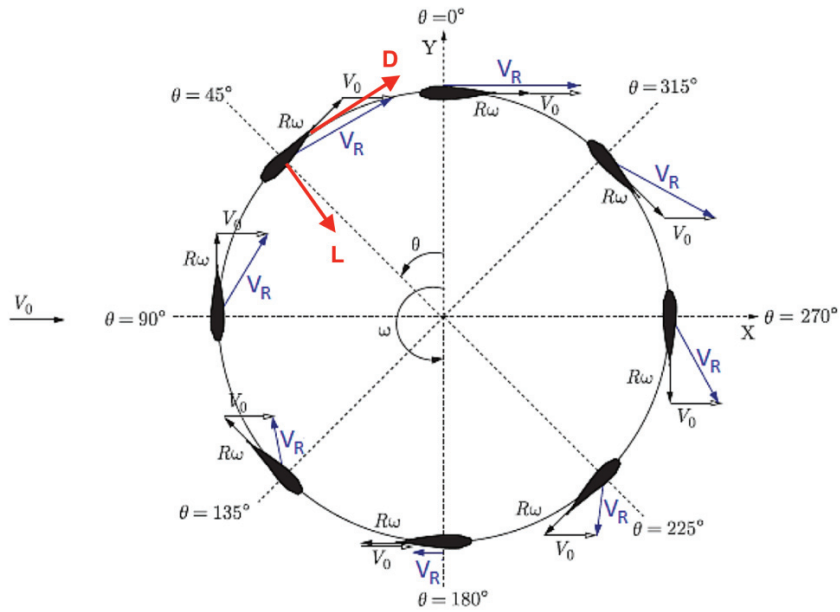

Figure 2.2 Velocity and Force Vectors applied on VAWT (*2*)

Both the relative velocity vector $(\overrightarrow{V_R})$ and angle of attack (α) are functions of the azimuth angle (θ) of the airfoil. Thus, the lift and drag forces depend on the azimuth angle of the airfoil of the VAWT. The operating tip speed ratio, also known as TSR (λ), is a significant parameter associated with VAWTs. Where the ω_r is the angular velocity (rad/s) and, R is the wind turbine radius (m).

$$\lambda = \frac{\omega_r R}{V_\theta} \tag{2.22}$$

The solidity (σ) is defined as the ratio of the frontal airfoil surface area to the swept area of the wind turbine that is covered by the airfoil blades.

$$\sigma = \frac{N_b c}{D} \tag{2.23}$$

$$\alpha = tan^{-1} \frac{cos\theta}{sin\theta + \lambda} \tag{2.24}$$

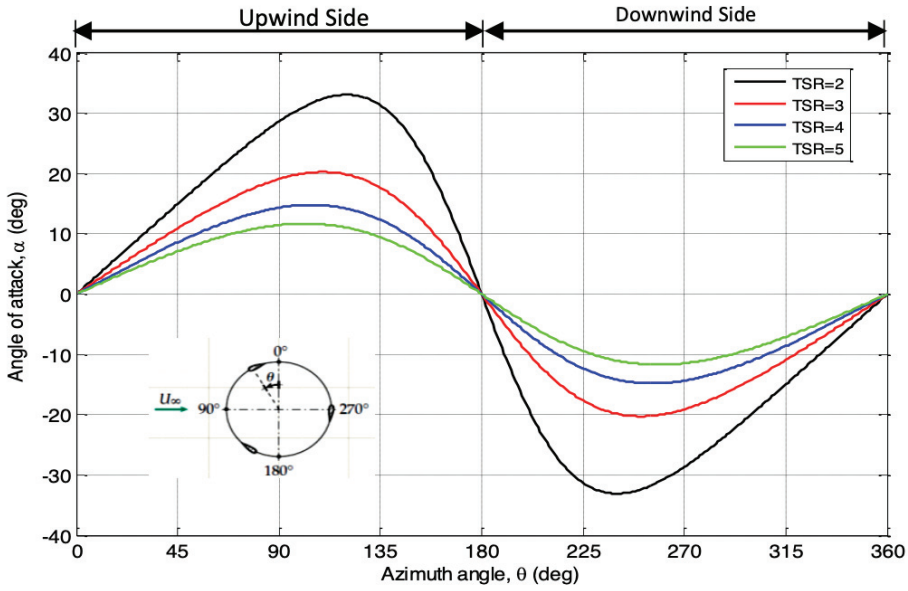

Figure 2.3 Typical changes in the angle of attack at a variety of TSRs *(4)*

As can be seen in Figure 2.3, the airfoil of the VAWT frequently exposes a high angle of attack that is greater than the expected stall angle when operating at low TSRs. This indicates that the airfoil is experiencing an extended period of stall condition during its one complete rotation compared to the high TSRs. Thus, the lift force and the torque of the turbine decrease rapidly while the drag force increases. Furthermore, the increase in the angle of attack of the airfoils in the turbine causes the formation of vortices on the upper side of the airfoils, which cause more turbulence in the flow *(3)*.

Performance parameters of the VAWT, drag coefficient (C_{Drag}) and lift coefficient (C_{Lift}) are given in the Equations 2.25 – 2.26, where ρ_a is the air density

(kg/m^3), A is the swept area by the turbine (m^2), τ_t is the rotor torque (Nm). The forces applied, the drag force (F_{Drag}) and the lift force (F_{Lift}), to the airfoil of the VAWT can be seen in Figure 2.2.

$$C_D = \frac{F_{Drag}}{0{,}5AV_R{}^2} \tag{2.25}$$

$$C_L = \frac{F_{Lift}}{0{,}5AV_R{}^2} \tag{2.26}$$

To normalize the forces acting on a blade, force coefficients can be used. The tangential force coefficients (C_t) and normal force coefficients (C_n) for each azimuthal position can be calculated using the equations below.

$$C_t = C_L \sin(\theta) - C_D \cos(\theta) \tag{2.27}$$

$$C_n = C_L \cos(\theta) + C_D \sin(\theta) \tag{2.28}$$

The following equation can be used to determine the turbine's torque (τ_t) (Nm). H represent height of the turbine. Once the turbine's torque has been calculated, both the moment coefficient (C_m) and the averaged moment coefficient ($C_{m,avg}$) of the turbine can be found easily.

$$\tau_t = \frac{N_b cHR}{2\pi} \int_0^{2\pi} \frac{1}{2} \rho V_R{}^2 C_t d\theta \tag{2.29}$$

$$C_m = \frac{\tau_t}{\frac{1}{2}\rho V_0{}^2 AR} \tag{2.30}$$

$$C_{m,avg} = \frac{Nc}{2\pi\rho R V_0{}^2} \int_0^{2\pi} \frac{1}{2} \rho V_R{}^2 C_t d\theta \tag{2.31}$$

The mechanical power (P_m) that the VAWT produce can be found with Equation (2.32), and the power coefficient (C_p) can be found with Equation (2.33).

$$P_m = \omega_r \tau_t \tag{2.32}$$

$$C_p = \frac{P_m}{P_W} = \frac{\omega_r \tau_t}{0{,}5\rho_a A U_\infty^3} = \frac{(0{,}5\rho_a A U_\infty^2 R) C_m \omega_r}{0{,}5\rho_a A U_\infty^3} = \frac{C_m \omega_r R}{U_\infty} = C_m \lambda \quad (2.33)$$

2.5. Simulation Settings

To be able to run simulations, many different configurations and settings must be adjusted. In this part, a summary of the simulation settings is given, along with descriptions where necessary. All simulations were 2D transient and a pressure-based solver is used. The k-ω-SST selected as turbulence model.

The simulation's parameters are displayed in Table 2.1. The dynamic viscosity of air is $\mu = 1.7894\ x\ 10^{-5} kg\ m^{-1} s^{-1}$, the air density is $1.225\ kg\ m^{-3}$, outlet pressure of the domain has been set to 101,325 pascal which is the ambient pressure. The temperature of the environment has been set to 300 K. As can be seen on Table 2.2, there are 3 simulation domains to calculate the performance of the VAWT.

Table 2.1 The simulation parameters of the CFD simulations

Setup	Type:	Pressure Based
	Time:	Transient
Boundary Conditions	Inlet:	
	Velocity Specification Method:	Components
	X-Velocity:	8 m/s
	Outlet: (Pressure Outlet)	
	Backflow Reference Frame:	Absolute
	Backflow Reference Specification:	Total Pressure
Cell Zone Conditions	Turbine Zone	
	Speed: (rad/s)	Depends on the TSR
	Air Foil Zone	
	Speed: (rad/s)	Relative to the Turbine Zone
	Fluid Domain	

As shown in Table 2.1, the simulation domain has been divided into three different zones; rotating rotor zone, stationary fluid zone, and airfoil zones. Because of all CFD simulations in this study based on the three different turbine models, 1-bladed, 2-bladed, and 3-bladed VAWT models, the number of airfoil zones varies for the CFD simulation of VAWT that working in pairs and standalone working VAWTs. The airfoil zone and rotor zone rotate at the same angular velocity, and the relative speed of the airfoil zone to the turbine zone is 0. Since the wind velocity in the x direction is considered to be constant, 8 m/s, in the reference studies, the RPM of the rotor zone was assumed to be variable for the CFD simulations at various TSRs. The RPM of the rotor zone at 1.7 TSR is 16 rad/s, at 2.2 TSR it is 20.7858 rad/s, at 3.3 TSR it is 30.0588 rad/s, and at 4.4 TSR it is 41.4117 rad/s. The moving mesh option has been selected for the two rotating zones so that the mesh is not regenerated at every step of the calculations.

As a solution method, the coupled algorithm was selected for simulations with the 2nd Order Upwind numerical schemes. The maximum iteration number was set to 20. According to experience gained, 20 iterations are enough to converge each iteration.

Table 2.2 Solution Settings of CFD simulation

Solver	Pressure-based with Coupled Algorithm
Numerical Schemes	2nd Order Upwind
Turbulence Model	k-ω Shear Stress Transport (SST)
Simulation Domain	Rotating Rotor Zone
	Stationary Fluid Zone
	Airfoil Zone

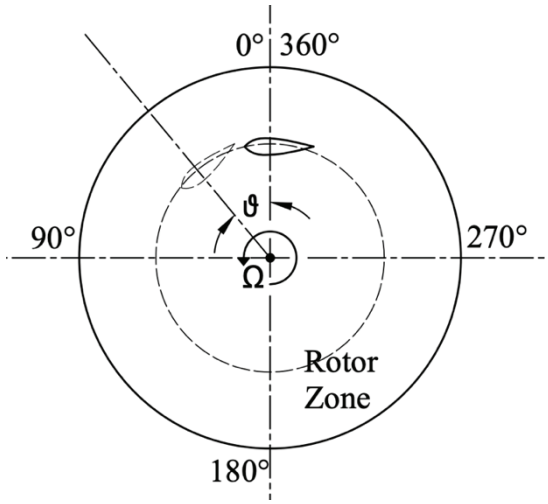

Figure 2.4 The position of the airfoil in relation to the azimuth angle on a turbine

In order to obtain more accurate and stable results from all simulations, the data of the 10 th revolution of the turbines was used to eliminate the turbulence that formed on the airfoil boundary layer at the starting phase of the turbine and to wait for the flow to stabilize on the turbine and its blades. Due to the fact that multiple azimuthal angle increments are used in the simulations, the time step size can be calculated using the equations below to prevent any confusion. Figure 2.4 shows the location of the blades and its azimuthal angle during full rotation.

$$NTS = N\frac{360}{\vartheta} \tag{2.35}$$

$$TSS = \frac{N}{(0.15915\omega)NTS} \tag{2.36}$$

TSS is the time step size in Equation 2.36, whereas N is the number of rotations and NTS is the number of time steps. The azimuthal angle of the turbine is denoted by ϑ, while the angular speed of the turbine is denoted by ω. The NTS, TSS in Equation 2.35. The values for each simulation are shown in the next chapter, which may be found in Table 2.4.

2.6. Geometric Properties of Simulation Domain

Figure 2.5 illustrates a schematic diagram of the simulation domain. The geometric properties of all simulation domain and its components are modeled based on Balduzzi et al.'s VAWT model (*11*). The left side of the fluid domain is set as a velocity inlet, $V_i = 8\ m/s$, while the right side is set as a pressure outlet $P_a = 101.325\ Kpa$. The upper and bottom sides of the fluid zone are set as non-shear walls. There is a turbine with three different designs that can be seen in the fluid zone called the rotor zone in the present study. The rotor zone is the rotation domain while rest of the fluid domain is stationary. The interface between the stationary domain and the rotating domain is modelled by the sliding mesh technic. Table 2.3 shows the detailed geometric properties of the simulation domain.

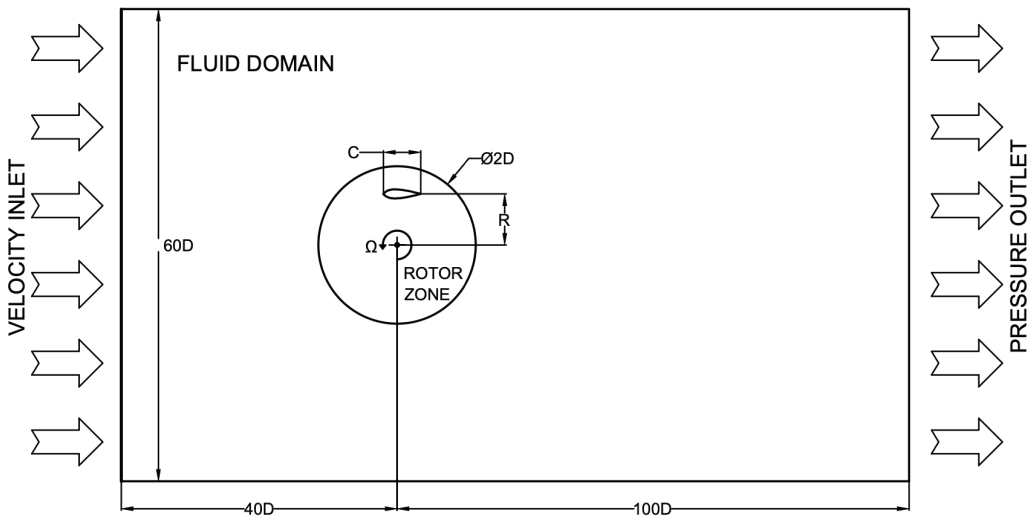

Figure 2.5 Schematic view of the simulation domain of the Vertical Axis Wind Turbine with 1-bladed turbine

It is crucial to have a big enough domain size to reduce the impact of blockage and uncertainties in the boundary conditions on the results when simulating the efficiency of a vertical-axis wind turbine using CFD simulations (*22*).

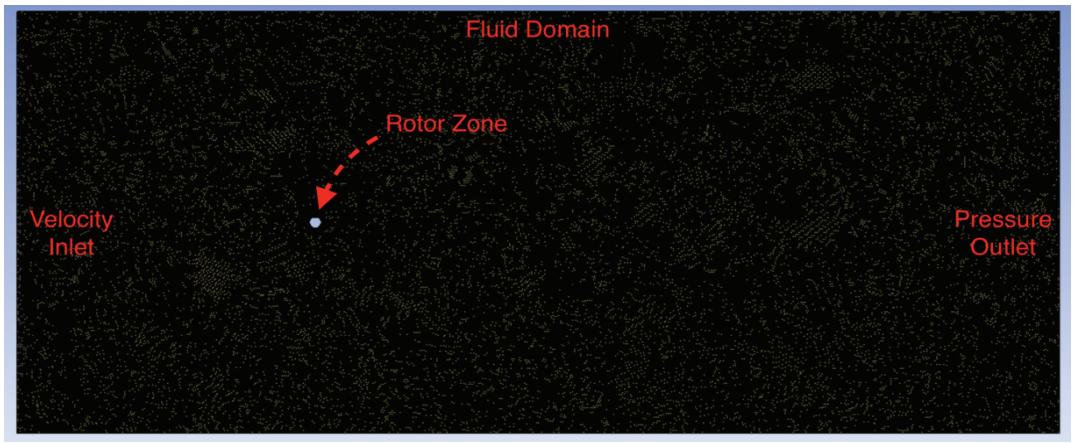

Figure 2.6 Mesh details of simulation domain

Table 2. 3 Geometric properties of the simulation domain

Airfoil		
	Type:	NACA0018
	Chord Length: (c)	0.246m
	Number of Blades:	Depends on Turbine Model
	Blade Shape:	Straight
Turbine Zone		
	Rotor Zone Diameter:	2600mm (2D)
	Turbine Radius: (R)	850mm
Airfoil Zone		
	Diameter:	350mm
	Zone Number:	Depends on Turbine Model
Fluid Zone		
	Length:	182000mm (140D)
	Height:	78000mm (60D)

Figure 2.6 shows the fluid domain that was used in the simulations. It can be seen that the fluid domain is significantly larger than the rotor zone to avoid the wind blockage. In CFD simulations, 3 different turbine models and co-rotaing turbines with various inter turbine distances used while the fluid domain stays the same. The schematic figure of

these three turbine model and co-rotating turbines are shown in Figure 2.7. The total mesh number of elements grow as the number of blades, airfoil zones, and interfaces of the blades increases. In order to achieve optimal and accurate results, the mesh sizes have been increased at the fluid domain even though that the fluid domain dimensions remain the same. Thus, the mesh number, the mesh sizes, and the mesh types in critical regions, such as the mesh in the airfoil zone, the mesh on the airfoil or blade boundary layers, and the mesh in the rotor zone have not been changed, while the mesh size in the fluid domain has been increased in the region that will have the least impact on the simulation results.

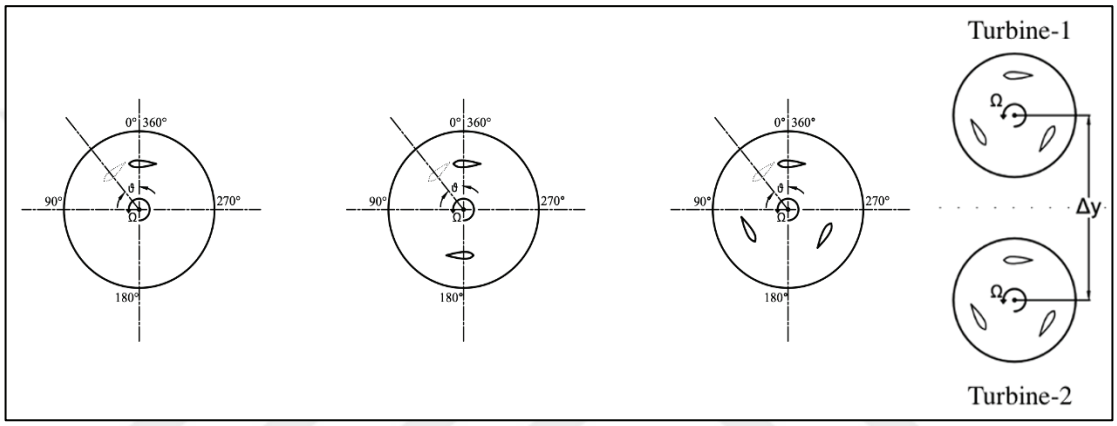

Figure 2.7 4-different turbine models A) 1-Bladed Turbine Model B) 2-Bladed Turbine Model C) 3-Bladed Turbine Model D) Co-Rotating Turbines

Figure 2.8 shows the detailed image of the airfoil for the finest mesh settings. A is the tip of the NACA0018 airfoil, B is the back of the NACA0018 airfoil and C is and the airfoil zone. Except for the mesh independency analysis, the finest mesh settings, detailed in Figure 2.8 were used for all simulations. A inflation mesh with a growth rate of 1.1 and a transition ratio of 0.2 with a maximum of 25 layers is used on the surface of the airfoil. The mesh element size in the airfoil zone is 1.2 mm with the 1 mm defeature size and finally the mesh number of division of the interface of the airfoil zone is 500.

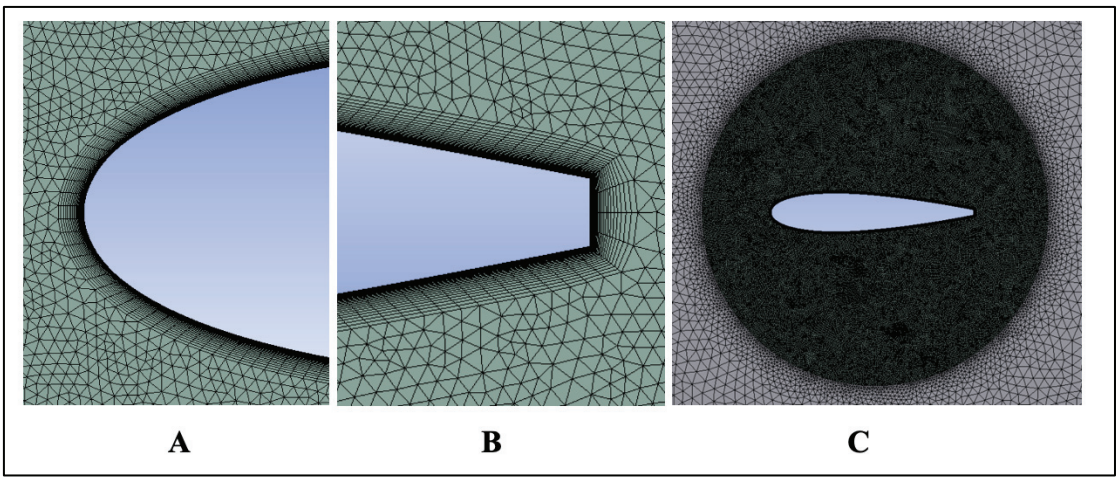

Figure 2.8 Mesh Details of Airfoil and Airfoil Zone A) Mesh details of tip of the NACA0018 profile airfoil B) Mesh details of the back of the NACA0018 profile airfoil C) Mesh details of airfoil zone

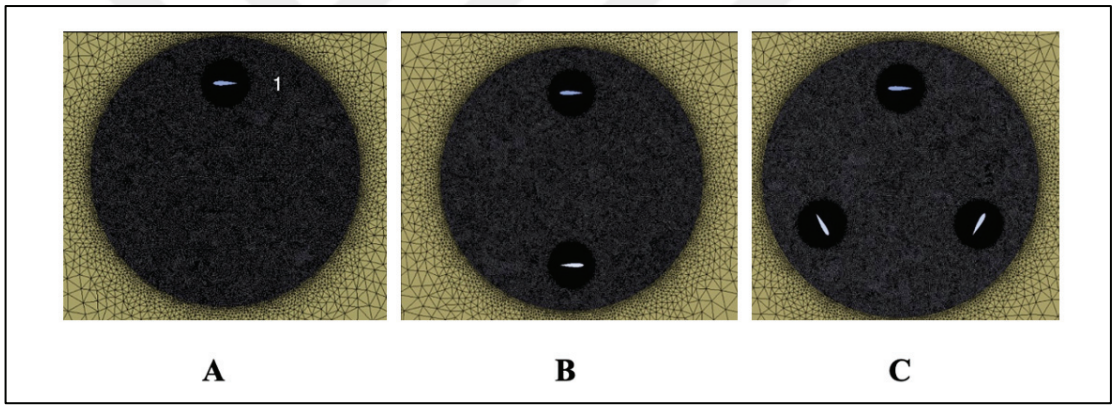

Figure 2.9 Mesh details of 3-different turbine models A) Mesh details of 1-bladed turbine B) Mesh details of 2-bladed turbine C) Mesh details of 3-bladed turbine

Figure 2.9 shows the mesh details of the turbines of the standalone VAWT. The purpose of these 3 different turbine models is to compare the aerodynamic effects of each blade to one another. The mesh element size of the rotor zone is 10 mm with a 8 mm defeature size for each of the three turbine models. The mesh number of division of the interface of rotor zone is 500.

2.7. CFD Simulations

2.7.1. Mesh Independency Analysis

When it comes to running simulations and getting accurate results from them, the mesh independency analysis is one of the most significant factors. It is a problem that demands further focus, and mesh independency analysis should be worked on separately from experimental studies. Due to their design, VAWTs are exposed to airflow from nearly all directions. In this scenario, the mesh structure has a significant impact on the results.

All of the CFD simulations were performed using the student version of the Ansys 2022 R1 software. However, due to the limitations of the student version of Ansys, the mesh sizes used in the simulations was restricted. Therefore, a mesh analysis could be performed on a maximum of 512000 mesh element numbers. Although creating a dense mesh structure as in the Balduzzi et al.' CFD simulations (*11*) is nearly impossible with the student version of software, accurate results can be obtained from CFD simulations within the mesh number limits. Since the fluid domain is substantially larger than the turbine zone and the mesh element numebr is limited, the highest mesh density is generated on the airfoil and on the turbine zone.

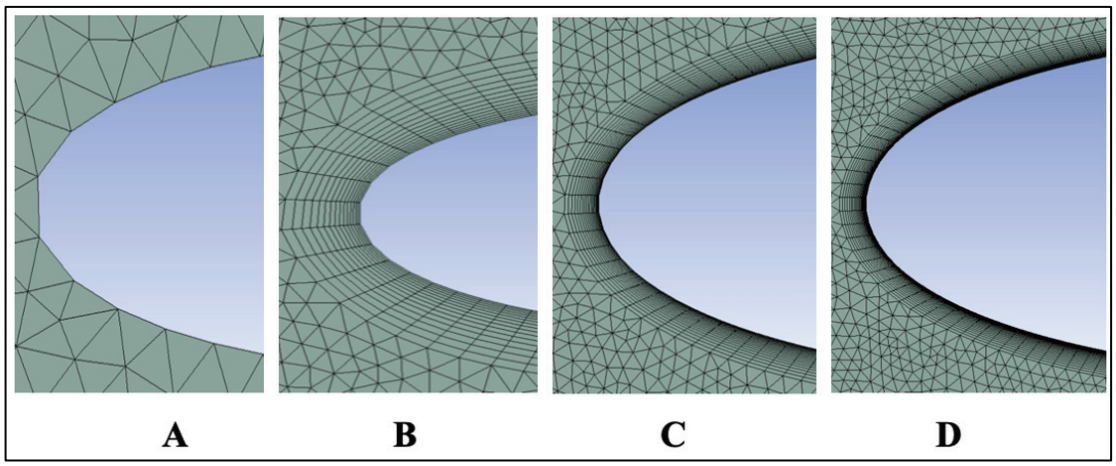

Figure 2.10 Mesh structures of the tip of the NACA0018 airfoil

Figure 2.10 shows the mesh details on the surface of the NACA0018 profile airfoil. As can be seen in the figure, the inflation mesh method was not used on the airfoil surface in the coarser mesh setting (A). As the mesh element number increases, the mesh

structure of the airfoil becomes finer. In the 2nd mesh setting (B), the inflation mesh method with a maximum layer of 15, a growth rate of 1.4, and a transition ratio of 0.4 have been added to the airfoil surface. While the maximum layer of the inflation mesh method on the airfoil has been increased to 15, the transition ratio and the growth rate have been reduced to 0.3 and 1.2 in the third mesh settings (C). Finally, in the fourth mesh setting (D) with 505K mesh element number, the maximum layer of the inflation mesh method applied to the airfoil surface is 25, the growth rate is 1.1, and the transition ratio is 0.2.

In order to analyze the mesh independency analysis of a standalone working VAWT, 16 CFD simulations in total were performed at 4 different TSRs (1.7 TSR, 2.2 TSR, 3.3 TSR, and 4.4 TSR), each with 4 different mesh settings. The moment coefficient results obtained from these CFD simulations were compared below.

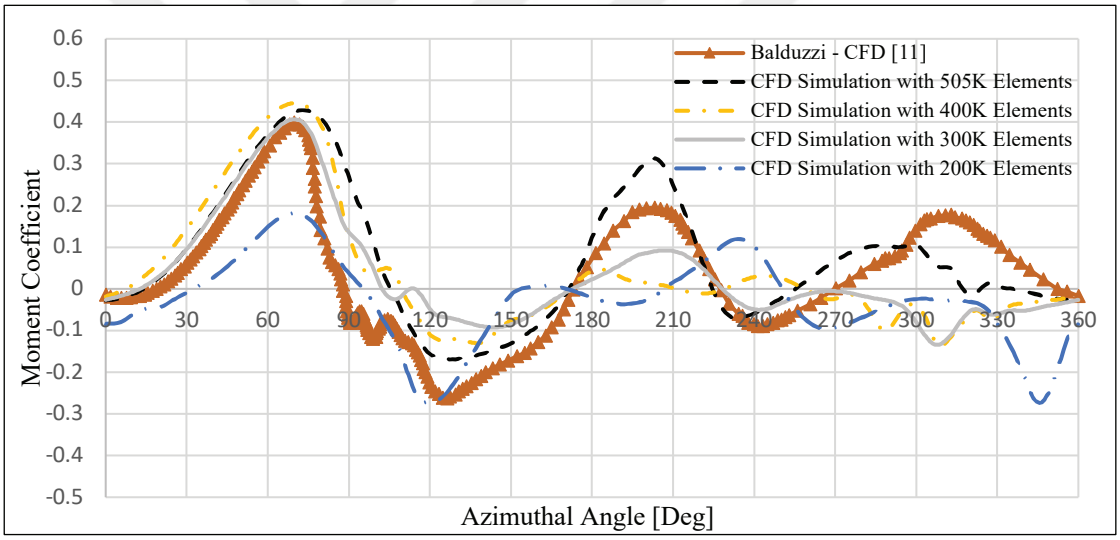

Figure 2.11 Mesh independency analysis at 1.7 TSR

The chart of moment coefficient obtained at 1.7 TSR for the four different mesh settings are significantly dissimilar, as shown in Figure 2.11. The simulation with the finest mesh structure, with a mesh element number of 505000, behaved almost identically to a two-bladed turbine, with a dramatic increase in moment coefficient after 180 degrees. Nonetheless, in the simulation with the coarser mesh and element numbers of 200000, it produced less moment coefficient than the others, with a sudden decrease after 330 degrees.

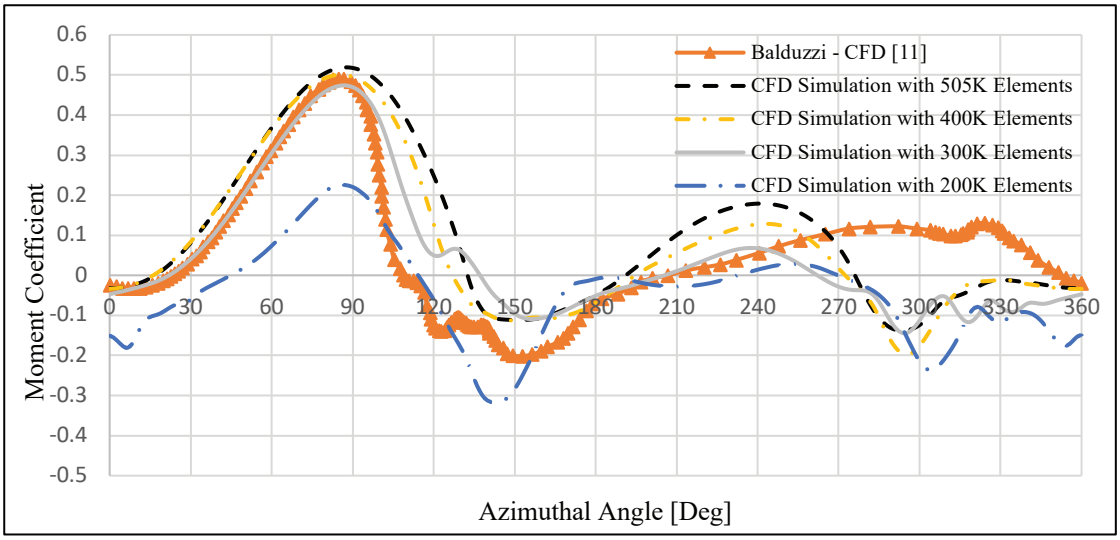

Figure 2.12 Mesh independency analysis at 2.2 TSR

Figure 2.12 shows that the results of the 4 mesh settings obtained from at 2.2 TSR. The results differ from each other, but not as much as at 1.7 TSR. As shown in the chart, the results of CFD simulations with the less mesh elements number produced the lowest moment coefficient during full rotation of the turbine.

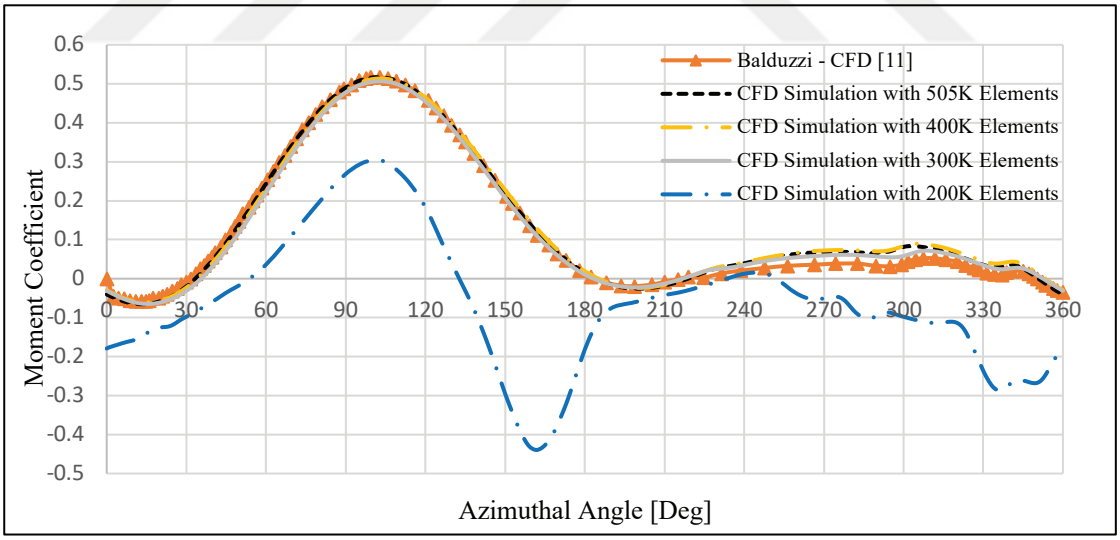

Figure 2.13 Mesh independency analysis at 3.3 TSR

Figure 2.13 shows the results obtained at TSR 3.3, the stable operating speed of the VAWT. Even though a difference of 100000 mesh elements number between each mesh setting, the results are similar at the TSR 3.3 except for the mesh setting where the influence mesh method was not applied on the airfoil surface.

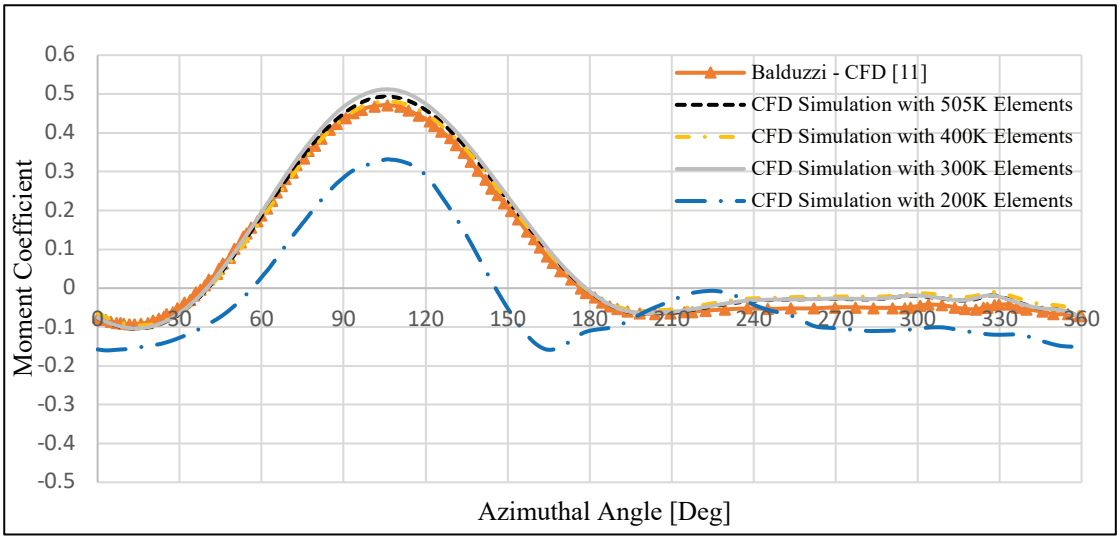

Figure 2.14 Mesh independency analysis at 4.4 TSR

Except for coarser mesh setting, simulation results with three different mesh settings are nearly identical at TSR 4.4, as shown in Figure 2.14. The results of 16 simulations in the mesh independency analysis show that changing the mesh element number size for the mesh independency analysis did not make a significant difference on the stable operating speeds of VAWT. In addition that the mesh methods make a bigger difference on the airfoil surface than the mesh elements number.

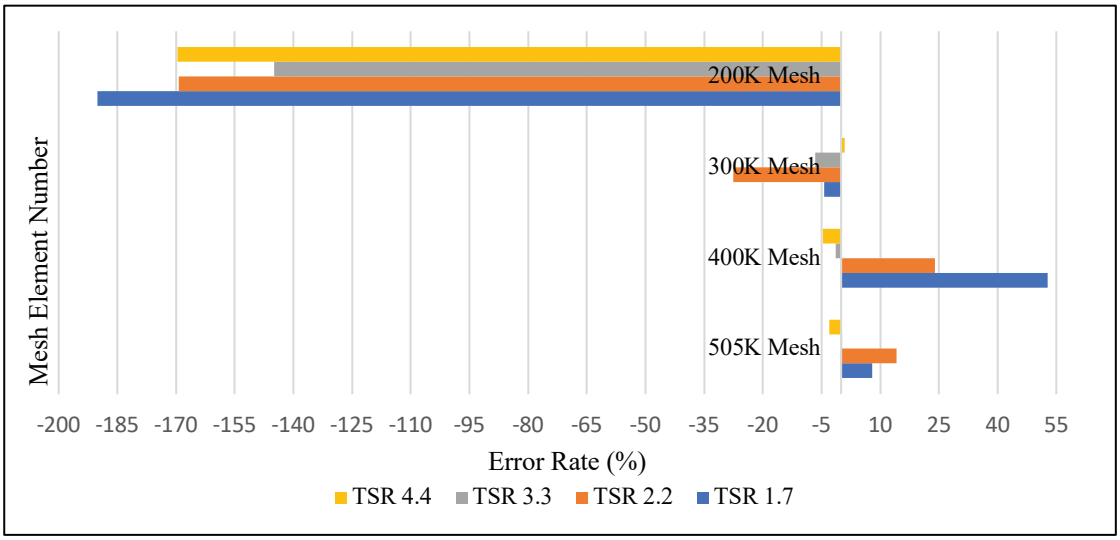

Figure 2.15 Error rates of mesh independency analysis

Finally, the average power coefficient values of simulations performed with mesh element numbers of 200K, 300K, 400K, and 505K, at TSRs of 1.7, 2.2, 3.3, and 4.4, were compared with the results of a reference study and the error rate was calculated for each

simulation settings. The error rate for each simulation is shown in Figure 2.15. At all TSRs, the error rate or error margin of CFD simulations with 200K mesh elements will be multiplied by a factor of two. It is necessary to remind the reader that although the number of mesh elements is low, the high error rate is due to the lack of inflation mesh on the boundary layer of an airfoil. At some TSRs, the error rate of CFD simulations with 300K mesh elements is less than 400K, which is also remarkable. Even at TSR 1.7, it is more accurate than the rest. Despite sudden fluctuations in the moment coefficient diagrams presented previously, the CFD simulation results with 505K mesh elements are the most accurate when all TSRs are considered. 7.94% in TSR 1.7, 14.08% in TSR 2.2, 1% in TSR 3.3, and 3% in TSR 4.4 is the error rate of CFD simulation with 505K mesh elements in terms of power coefficient compared to a reference study.

2.7.2. Time Step Sensivity Analysis

To achieve accurate results in CFD simulations, it is necessary to ensure that the results are not affected by the time step size. Hence, in this chapter, the comparison of results will be carried out using time step sizes where a complete rotation of the VAWT corresponds to azimuthal increments of 0.25, 0.5 degree. The values of azimuthal increments, angular velocity, time step size, number of rotations, and number of time steps for various TSRs are shown in Table 2.4.

The angular velocity is set to 16 rad/s to perform the VAWT at TSR 1.7. The moment coefficient values are shown in Figure 2.16 for azimuthal angle increments of 0.25° which corresponds to a time step size of $0.0002727s$ and azimuthal angle increments of 0.5° which corresponds to a time step size of $0.00054543s$. Figure 2.20 demonstrates the power coefficient values obtained from CFD simulations of a VAWT operating at TSR 2.2. The figure shows that the averaged power coefficient value with 0.25° azimuthal angle increments is 0.054 and the power coefficient value with 0.5° azimuthal angle increments is 0.062. The chart shows a 13% difference between the two time step sizes.

Table 2. 4 Time steps for time step sensitivity analysis

TSR	Azimuthal Increments (Degree)	Angular Velocity (rad/s)	Time Step Size (s)	Number of Rotation	Number of Time Step
1.7	0.5	16	0.00054543	10	7200
	0.25	16	0.0002727	10	14400
2.2	0.5	20.7858	0.00041985	10	7200
	0.25	20.7858	0.00021073	10	14400
3.3	0.5	31.0588	0.00028098	10	7200
	0.25	31.0588	0.00014049	10	14400
4.4	0.5	41.4117	0.00021074	10	7200
	0.25	41.4117	0.00010537	10	14400

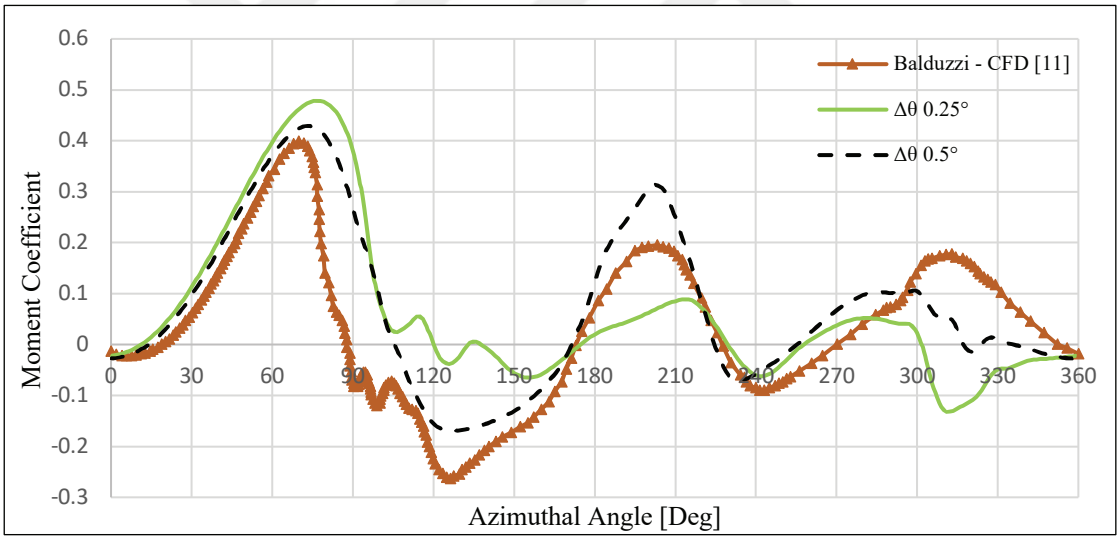

Figure 2.16 Time step sensitivity analysis at TSR 1.7

The angular velocity is set to 20.7058 rad/s to perform the turbine at TSR 2.2. The moment coefficient values are shown in Figure 2.17 for azimuthal angle increments of 0.25° which corresponds to a time step size of 0.000210736s and azimuthal angle increments of 0.5° which corresponds to a time step size of 0.00041985s. According to Figure 2.20, there is a %14.55 difference in the averaged power coefficient values obtained from CFD simulations using 0.25° and 0.5° azimuthal angle increments.

However, this difference can be considered negligible since the simulation using 0.25° azimuthal angle increments takes more than twice as much time as the simulation using 0.5° azimuthal angle increments.

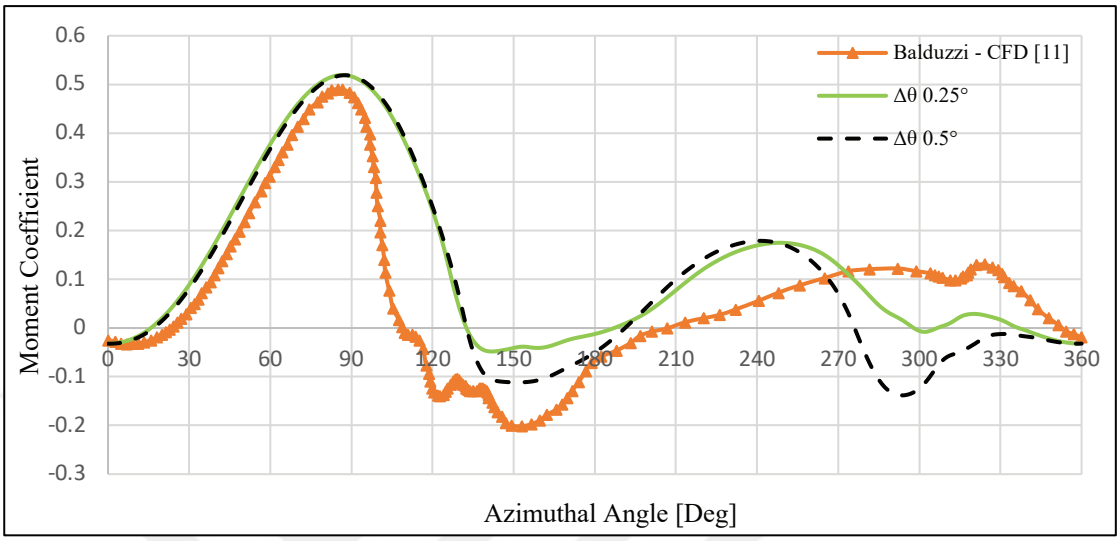

Figure 2.17 Time step sensitivity analysis at TSR 2.2

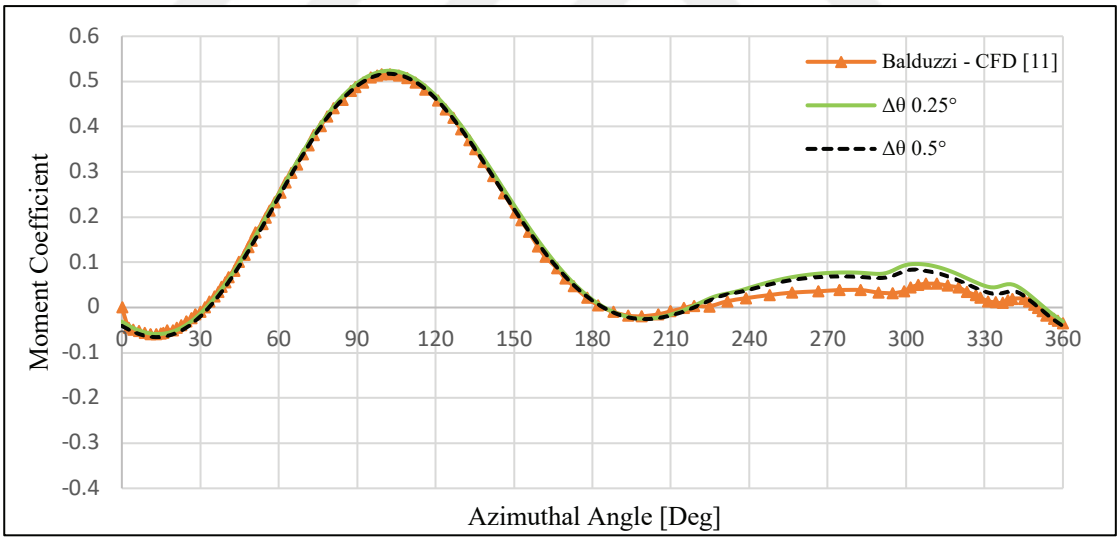

Figure 2.18 Time step sensitivity analysis at TSR 3.3

To operate the VAWT at TSR 3.3, the angular velocity was increased to 31.0588 rad/s. Figure 2.18 shows the moment coefficient chart obtained from CFD simulations with time step sizes of $0.00028098s$ and $0.00014049s$, corresponding to azimuthal angle increments of 0.25° and 0.5°, respectively. The averaged power coefficient value in Figure 2.20 is 0.459 for 0.25° increments and 0.435 for 0.5° increments, with a difference of %5.

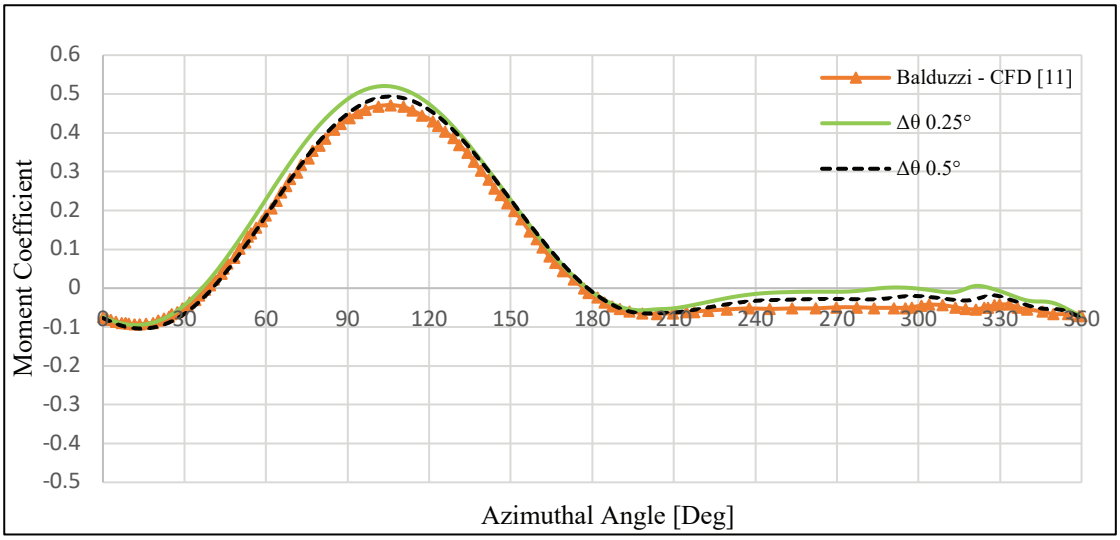

Figure 2.19 Time step sensitivity analysis at TSR 4.4

The VAWT was operated at TSR 4.4 by increasing the angular velocity to 41.4117 rad/s. The moment coefficient values obtained from CFD simulations with azimuthal angle increments of 0.5° which corresponds to a time step size of 0.00021074s and 0.25° which corresponds to a time step size of 0.00010537s are presented in Figure 2.19. Figure 2.20 shows that the averaged power coefficient value for 0.25° increments is 0.44, while the value for 0.5° increments is 0.37, resulting in a difference of %15.

The results obtained from the mesh independency analysis and time step sensitivity analysis were used to compare moment coefficient values obtained from 1 full turn of VAWT in various conditions through CFD simulations. Based on the analysis, it was found that using the finest mesh settings and a time step size corresponding to 0.5 azimuthal angle increments provided an optimal balance between the accuracy and computational cost of CFD simulations. With these mesh settings and parameters, averaged power coefficient values obtained from CFD simulations of a 1-bladed VAWT operating at various TSRs were compared with the reference study and validated.

The results of the Cp vs TSR chart with a 10% error bar in Figure 2.21 showed that the results obtained from the CFD simulations were nearly identical when compared with the reference study.

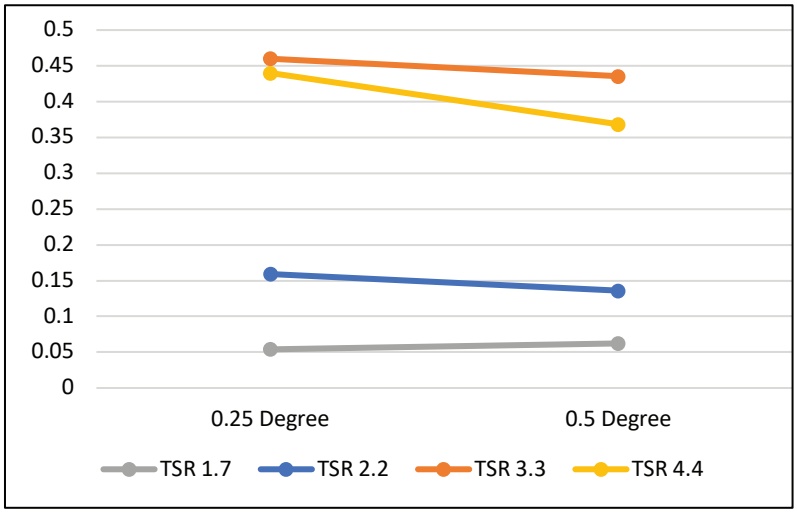

Figure 2.20 Time step sensitivity analysis at various TSR

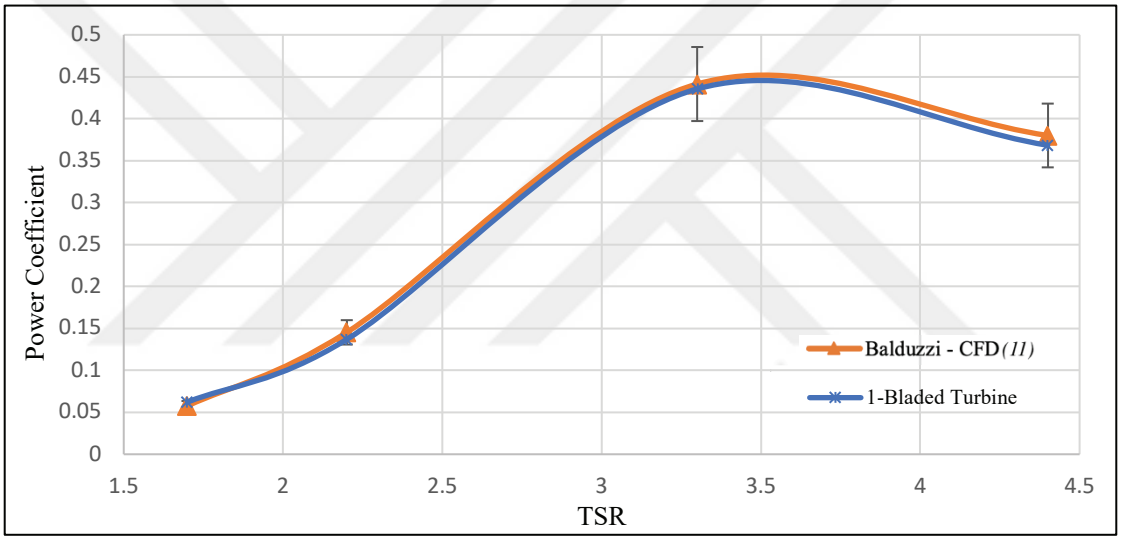

Figure 2.21 Comparison between CFD simulations and reference study for the 1-bladed turbine model: Cp vs. TSR

CHAPTER 3

RESULTS AND DISCUSSION

3.1. Standalone Vertical Axis Wind Turbine

To better understand the flow characteristics of a VAWT, a simulation of moment coefficient vs. blade angular position over a revolution was performed at various TSRs obtained by changing the rotational speed of the turbine under constant flow angle and constant flow velocity. For the standalone working turbine, the required time step size and turbine rpm values are given in Table 3.1.

Table 3.1 Tip Speed Ratio Table

Tip Speed Ratio	R (m)	Flow Velocity (m/s)	ω (rad/s)	Time step size (s)
1.7	0.85	8	16	0.000545432
2.2	0.85	8	20.7058	0.000421472
3.3	0.85	8	31.0588	0.000280981
4.4	0.85	8	41.4117	0.000210736

Figures 3.1, 3.2, and 3.3 show the graphs of the moment coefficient obtained from the blades at 0° position for 1-bladed, 2-bladed and 3-bladed turbine models for which CFD simulations were performed at four different TSRs. As seen in the graphs, the one-bladed turbine is unstable than the other two turbine models. As the number of turbine blades increases, the peak point of the moment coefficient values of the blade at 0 degrees decreases and the turbines are getting more stable. This is related to the solidity of the VAWT, which is defined as the ratio of the blade area to the swept area of the rotor. As the number of blades increases, the solidity also increases. This increased solidity improves the stability of the VAWT, but it also creates a wake flow behind each blade, leading to a reduction in overall performance. Therefore, even though the 3-bladed turbine model is the most stable, it has the lowest average power coefficient among the different blade configurations.

As shown in Figure 3.1, the stability of the turbine decreases as the TSR of the one-bladed turbine decreases. This phenomenon is caused by the development of a vortex on the boundary layer of the VAWT's blade when it operates at a low TSR. As the TSR of the turbine increases, the vortex formed on the blade boundary layer disappears, leading to improved stability of the turbine.

The one-bladed turbine reaches its highest moment coefficient value when operating at TSR 3.3 (Figure 3.1) whereas the two-bladed and three-bladed VAWTs reach their highest coefficient value at TSR 1.7 (Figure 3.2-3.3).

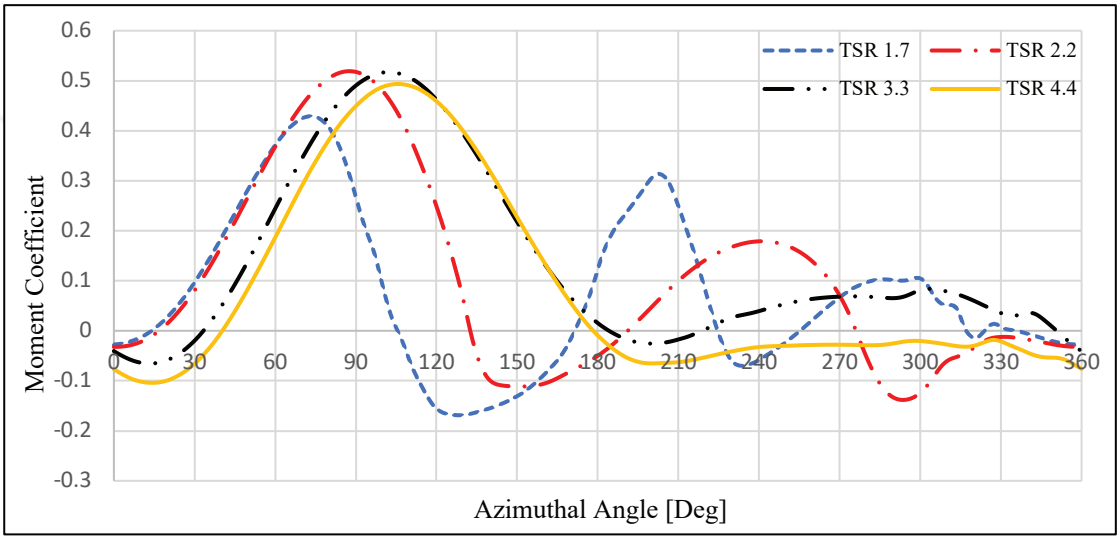

Figure 3.1 Moment Coefficient graph for 1-bladed turbine at different TSR values of 1.7, 2.2, 3.3 and 4.4

If we divide the azimuthal position of the turbine into 4 quarters to make the charts in Figure 3.1, Figure 3.2 and Figure 3.3 easier to understand, we can see that the one-bladed turbine operating at TSR 1.7 reached its maximum moment coefficient in the 1st quarter and a negative moment coefficient was observed in the 2nd quarter. The moment coefficient increased by 0.3 during the third quarter before falling back to a negative value. The reason for this fluctuation in the moment coefficient is caused by the development and shedding of the vortex on the blade surface as the turbine rotates as mentioned above.

When one more blade was added to the turbine, the negative moment coefficient in the 2nd quarter increased due to the increased solidty of the turbine and counterbalance

of the second blade.When the number of blades was increased to 3, the turbine reached its most stable state, but the maximum moment coefficient value decreased by 0.35.

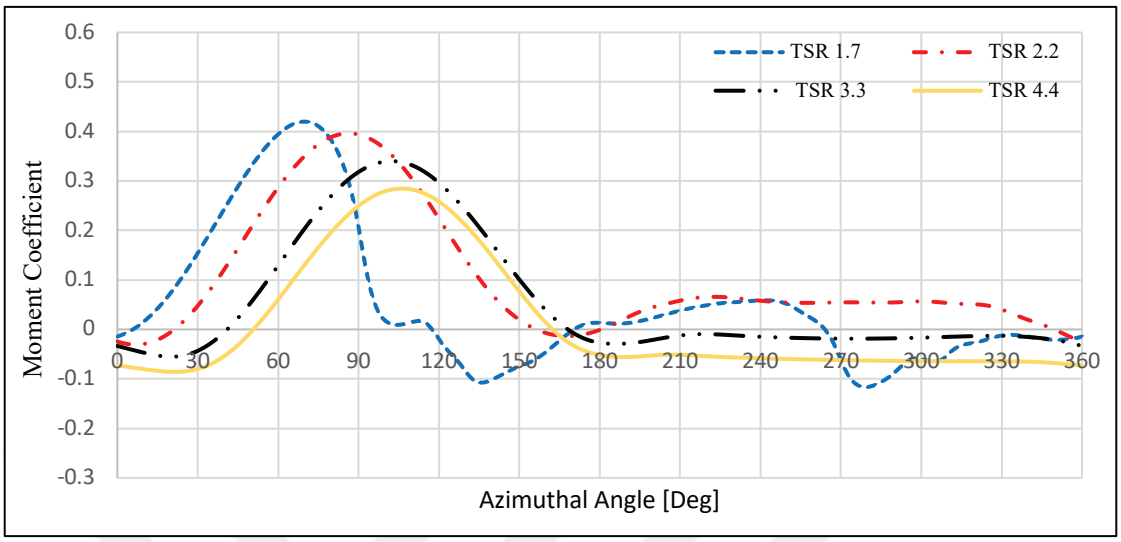

Figure 3.2 Moment Coefficient for 2-bladed turbine at different TSR values of 1.7, 2.2, 3.3 and 4.4

The one-bladed turbine reaches its maximum moment coefficient at 90 degrees when operating at TSR 2.2, and in the middle of the 3rd quarter, it reaches a moment coefficient of 0.2. At the end of the 2nd quarter and the beginning of the 4th quarter, the moment coefficient value becomes negative. The fluctuation in the moment coefficient at 2.2 TSR primarily due to two reasons. Firstly, the operating speed of TSR 2.2 is still unstable, which results in the vortex observed on the blade. Secondly, the one-bladed turbine with the lowest solidity exhibits the lowest stability, which further contributes to the fluctuation in the moment coefficient. As more blades are added, the moment coefficient of the VAWT becomes more stable and positive in all quarters. However, the maximum value of the moment coefficient decreases with the addition of each blade.The moment coefficient of the one-bladed turbine is stable when operating at TSR 3.3 and TSR 4.4. Adding more blades increases the stability of the moment coefficient, but as previously observed, the maximum moment coefficient decreases.

As illustrated in Figure 3.4, the highest power coefficients are obtained by the two-bladed and three-bladed turbines at the TSR 2.2, whereas the one-bladed turbine produces the highest power coefficient at TSR 3.3. Therefore, it can be concluded that increasing the number of blades in a turbine operating at high TSR leads to a decrease in power output due to the turbine solidity.

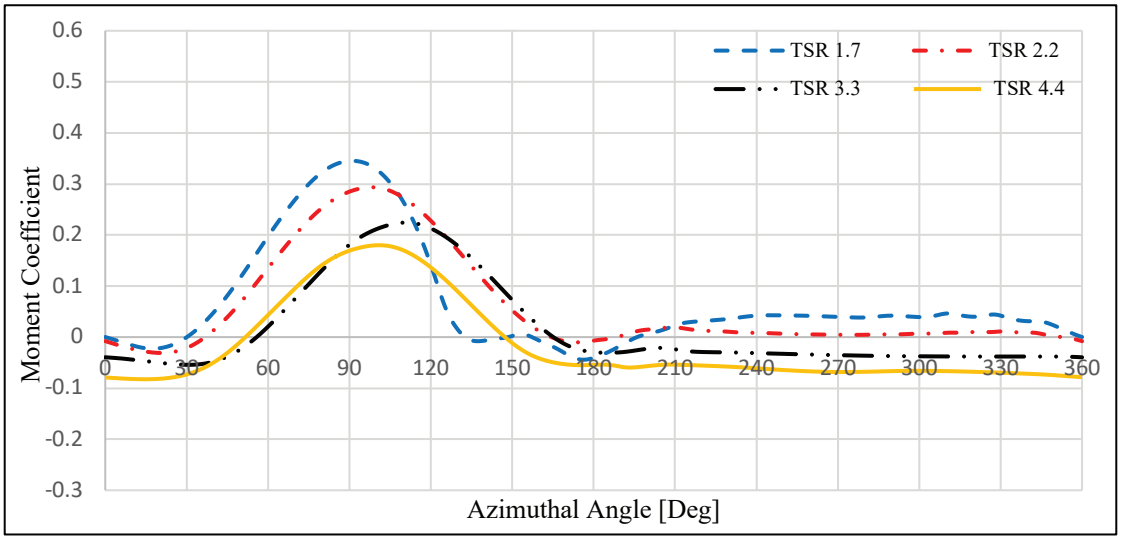

Figure 3.3 Moment Coefficient for 3-bladed turbine at different TSR values of 1.7, 2.2, 3.3 and 4.4

Since the freestream velocity was kept constant while adjusting the turbine RPM to change the TSR, as the turbine RPM was increased to operate at a higher TSR, the interaction of the blades with the wake flow in the turbine increased with each blade added, leading to a reduction in turbine efficiency at high TSR.

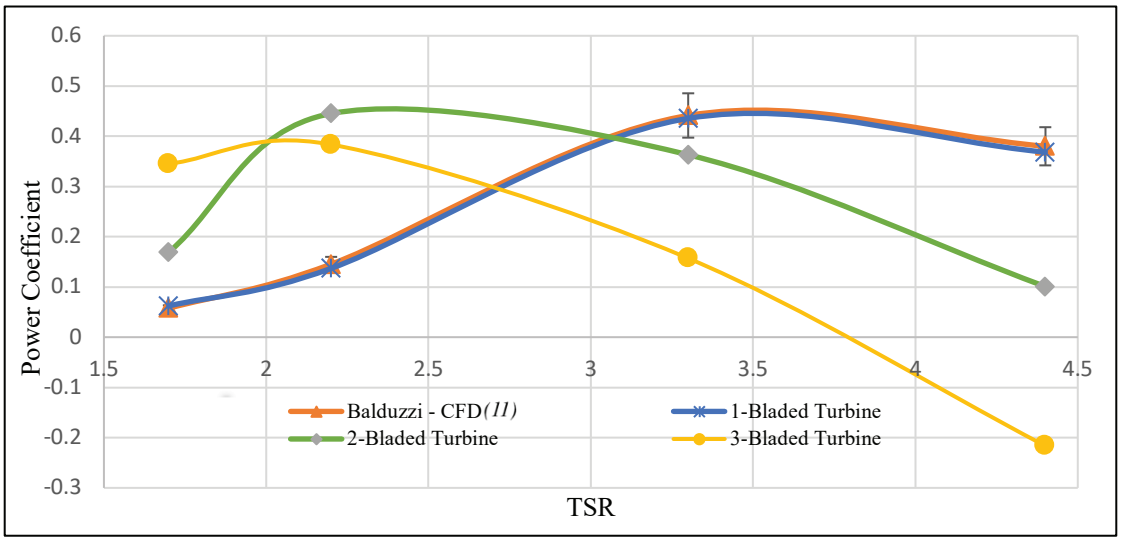

Figure 3.4 Comparison between CFD simulations and published studies for the 3 different turbine model: Cp vs. TSR

The figures below provide a clearer observation of how the turbine's performance is impacted by the vortex formation on the boundary layer of the turbine's blades when operating at low TSR and the turbine's solidity, as previously mentioned.

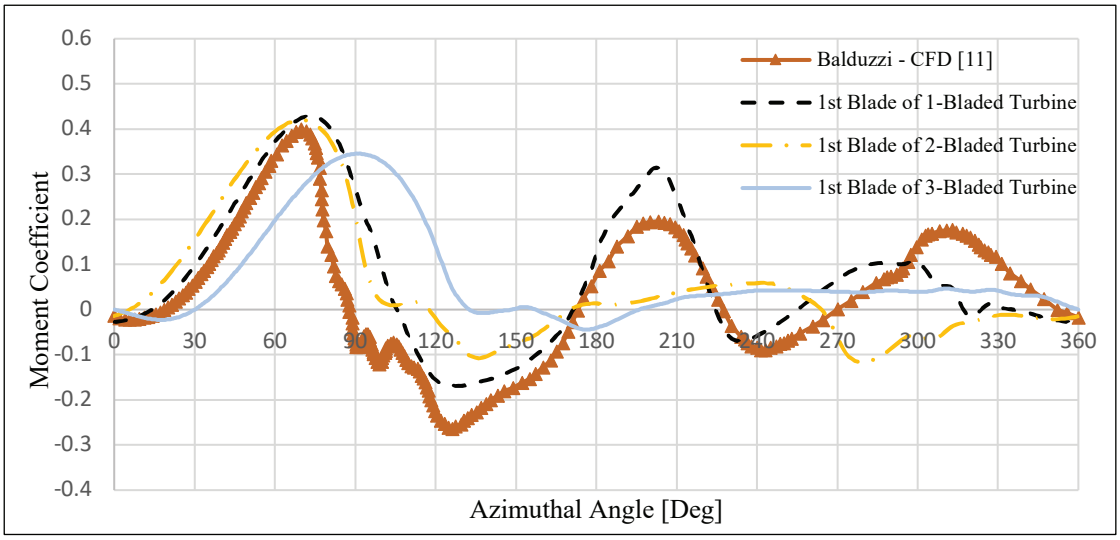

Figure 3.5 Moment Coefficient at 1.7 TSR

In Figure 3.5, the moment coefficient values obtained from 1 full rotation of the VAWT using 3 different turbine models operating at TSR 1.7 are compared. It can be seen that the VAWT becomes more stable as the number of blades in the turbine increases. Figure 3.6 shows the velocity counters of three different models of VAWTs at the same position while operating at TSR 1.7. The stability of a VAWT improves as the number of blades increases. However, with an increase in the number of blades, the permeability of the turbine decreases, causing a reduction in the freestream velocity and wake flow within the turbine. Nevertheless, each additional blade creates an individual wake flow to the blade behind.

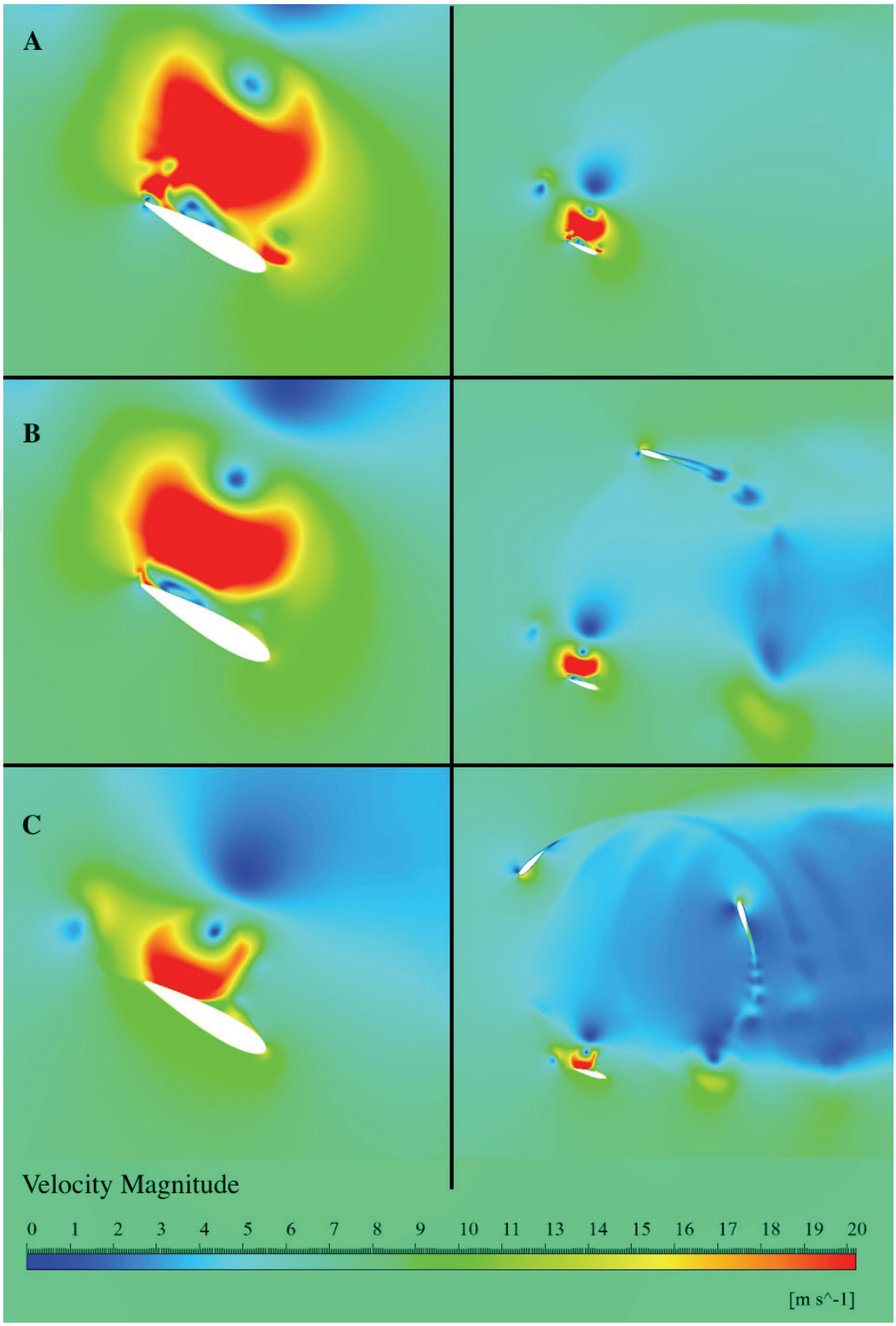

Figure 3.6 Velocity counters at $\theta = 160°$ for the 3 different VAWT models and their first blades operating at 1.7 TSR A) One-bladed VAWT B) Two-bladed VAWT C) Three-bladed VAWT

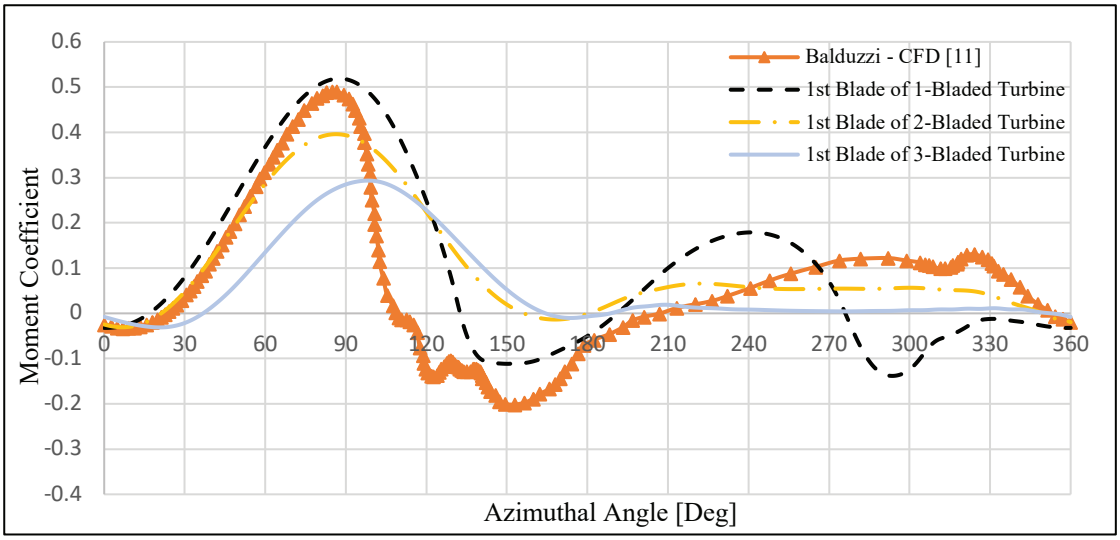

Figure 3.7 Moment Coefficient at 2.2 TSR

Figure 3.7 shows the moment coefficient values of VAWT with 3 different turbine models operating at TSR 2.2. As illustrated in the chart, TSR 2.2 remains an unstable operating speed, but the stability of VAWT increases with the addition of more blades. However, as the stability of VAWT increases, the maximum moment coefficient value it reaches decreases.

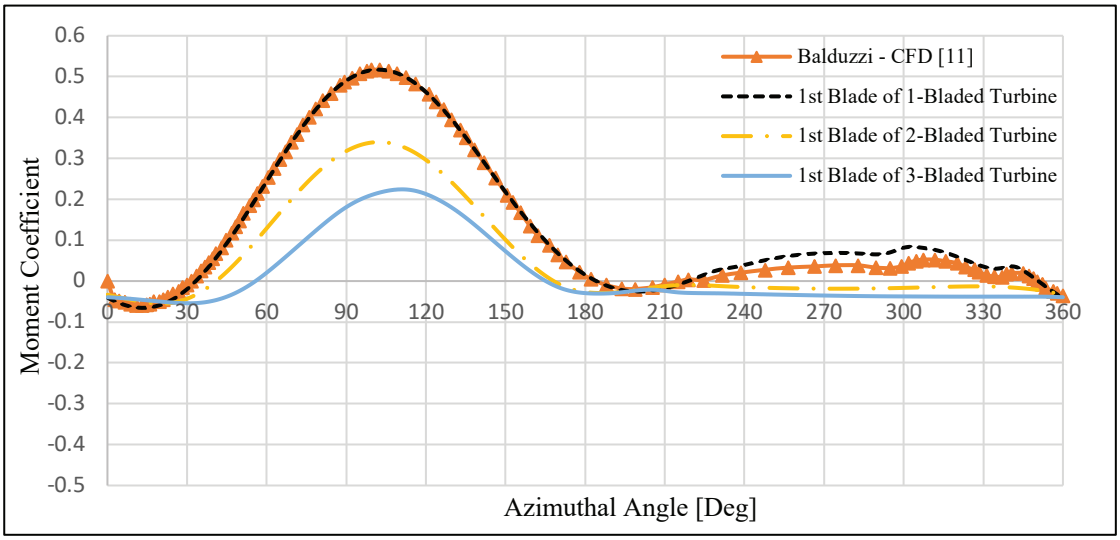

Figure 3.8 Moment Coefficient at 3.3 TSR

Figure 3.8 and Figure 3.10 show that the impact of higher solidities on VAWTs' performance is more noticeable when VAWTs with more blades operate at already stable and high TSRs. At TSR 3.3 and TSR 4.4, the maximum moment coefficient values

achieved by the VAWTs decrease as the number of blades increases. Moreover, with the increase in the number of blades, VAWTs generate negative moment coefficients, except between 30 and 180 degrees. Figure 3.9 shows the velocity counters of three different models of VAWTs that all operate at a stable TSR such as TSR 3.3. Due to the stable operating TSR, there is no vortex formed on the boundary layer of the blades. As can be seen in the figure, with the addition of each blade and increased angular velocity to operate the VAWTs at TSR 3.3 the VAWTs are able to operate at TSR 3.3, create wake flow for each blade and increase the interaction of the blades with the wake flow.

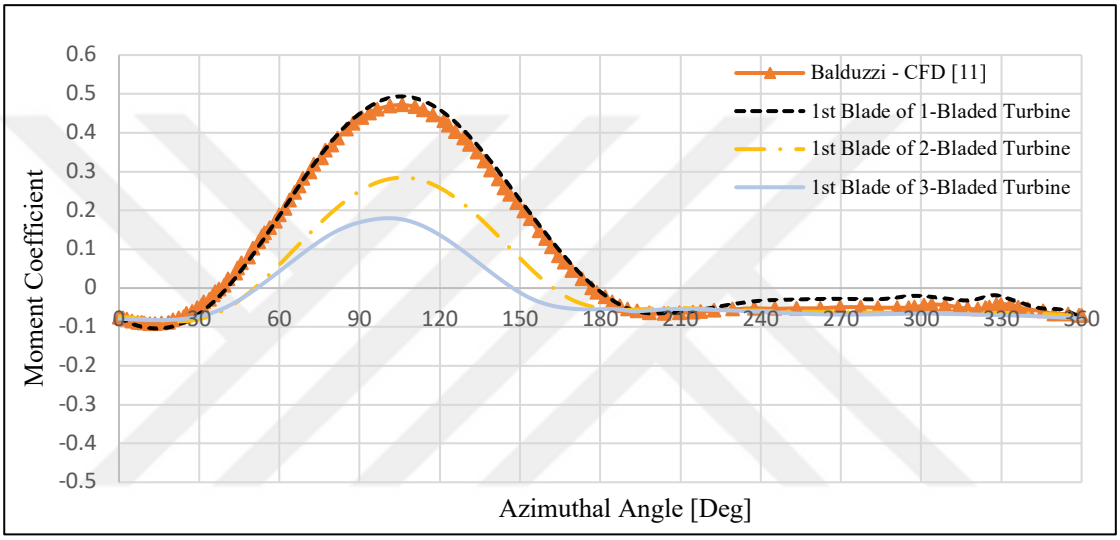

Figure 3.9 Moment Coefficient at 4.4 TSR

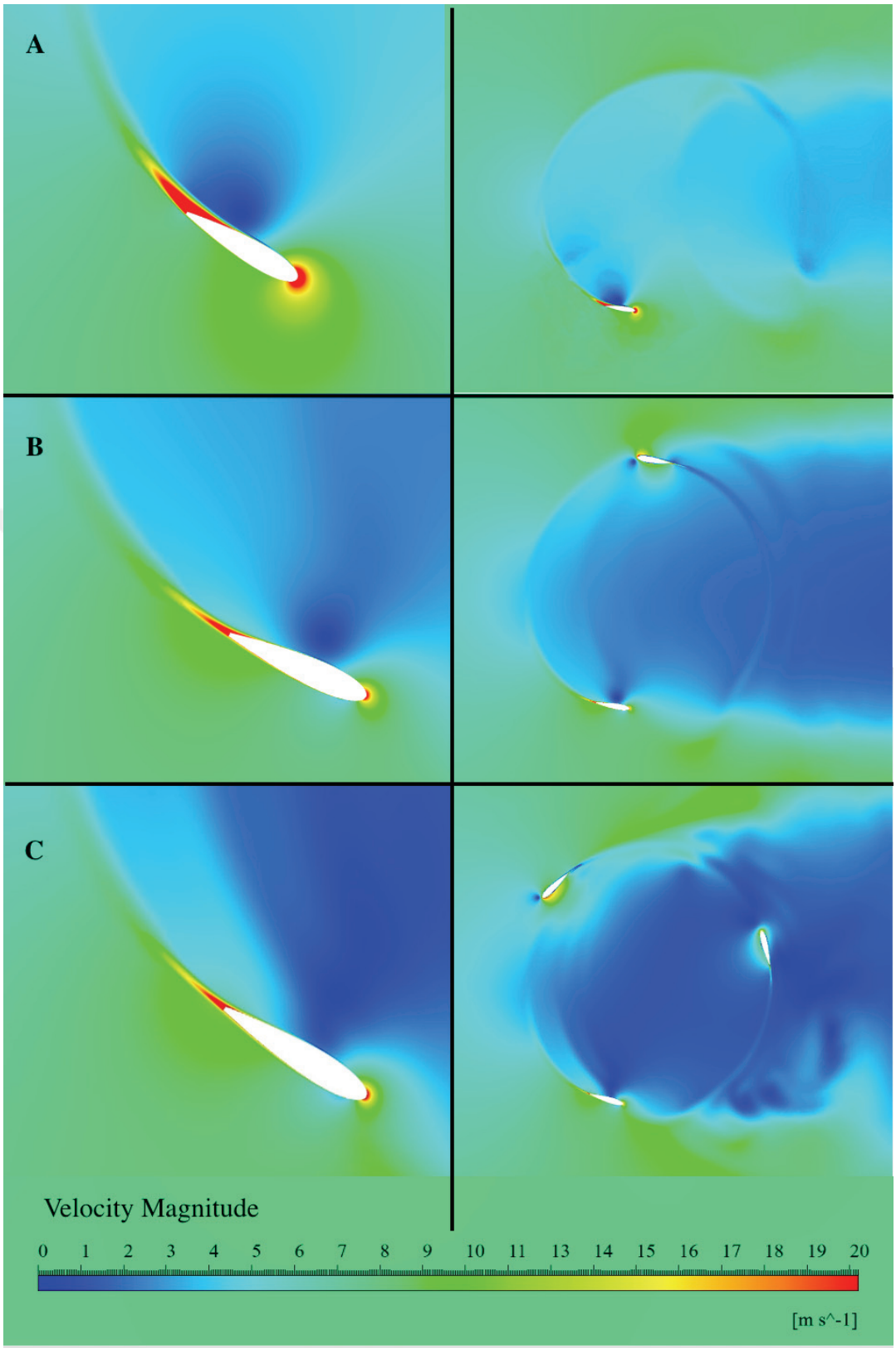

Figure 3.10 Velocity counters at $\theta = 160°$ for the 3 different VAWT models and their first blades operating at 3.3 TSR A) One-bladed VAWT B) Two-bladed VAWT C) Three-bladed VAWT

3.2. Results of Vertical Axis Wind Turbines That Working in Pairs

In this chapter, the effects of distance between the turbines are investigated by comparing the results of CFD simulations of VAWTs located at various distances with the CFD simulation results of the standalone VAWT with the same fluid domain.
In order to achieve this, simulation parameters from Table 2.1, simulation settings from Table 2.2, and geometric properties from Table 2.3 are used. Furthermore, the three-bladed turbine models shown in Figure 2.7 are used as a reference model for the investigation of the distance between blades' effects on turbine performance. Figure 3.11 shows the schematic view of the standalone VAWT and a pair of VAWTs that are positioned Δy apart from each other. In comparison to the reference studies in this section as references, the VAWT's two turbines rotate in the same direction, that is counterclockwise for each configuration. As previously stated, two VAWTs were located at varying distances (3D, 4D, 6D, 8D, 10D) and CFD simulations were made to analyze their performance at various TSRs (TSR 1.7, TSR 2.2, TSR 3.3, and TSR 4.4).

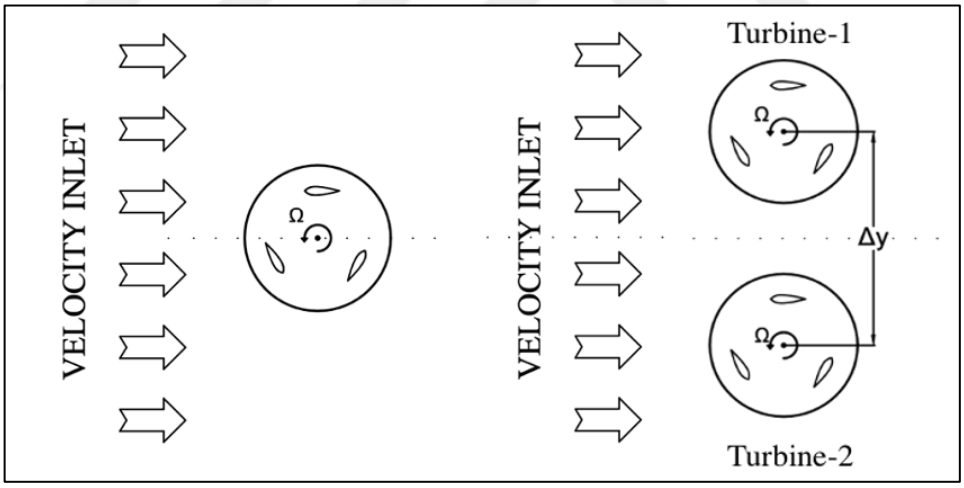

Figure 3.11 Schematic view of the standalone working VAWT and a pair of VAWTs that are positioned Δy apart from each other

The chart in Figure 3.12 shows the variation of the moment coefficient with the azimuthal angle of the two turbines positioned at varios distances from each other at TSR 1.7. The performance of the turbines is affected by their position. As the volume between two VAWTs decreases, the stream-tube effect became apparent in between VAWTs.

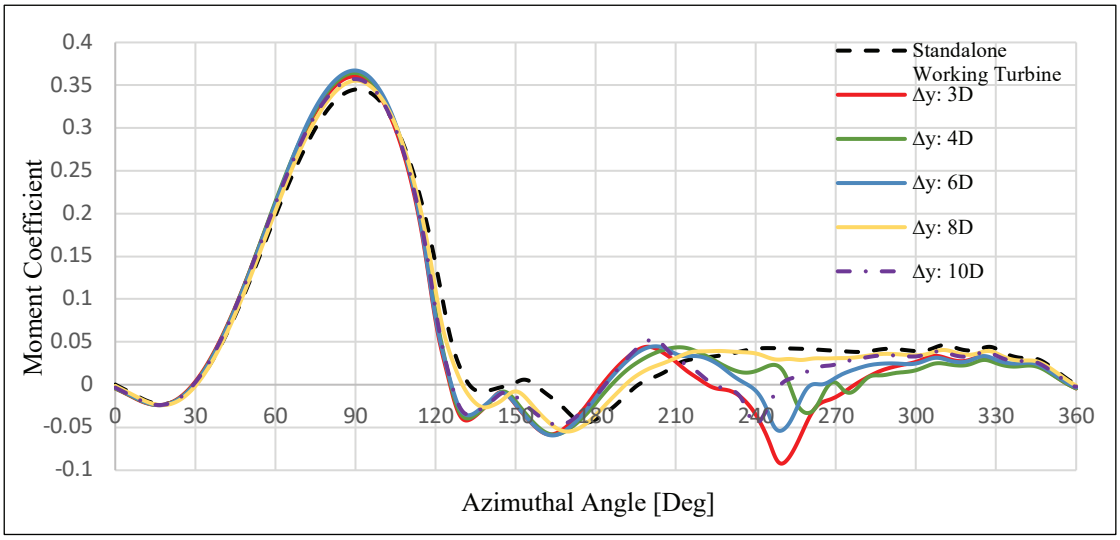

Figure 3.12 Instantaneous one-blade Cp for the Vertical Axis Wind Turbines working in pairs, compared to the isolated turbine at TSR 1.7

VAWTs operating at unstable TSRs negatively affect each other's performance due to the changes in the drag/lift force ratio caused by the stream-tube effect. Therefore, a decrease in the performance of operated VAWTs at unstable TSRs was observed. As the distance between VAWTs increases, the effect of the pressure zone or stream-tube effect between VAWTs decreases, and the reduction in performance becomes less significant. Finally, the performance of the VAWTs that were placed at distances of 3D, 4D, 6D, 8D, and 10D between each other was lower than that of a standalone turbine, with average power coefficient reductions of 12.61%, 10.44%, 13%, 6.9%, and 10%, respectively.

Figure 3.13 shows that VAWTs operating at TSR 2.2 and positioned at 3D, 4D, 6D, 8D, and 10D distances from each other have the same instantaneous moment coefficient values as the standalone turbine during the VAWTs' one full turn. However, as shown in Figure 3.16, the co-rotating turbines at TSR 2.2 generated a higher average power coefficient than the standalone turbine. According to the results of the CFD simulations, the co-rotating turbines worked best when they have placed 6D away from each other at TSR 2.2. Up to 6D distance, the power coefficient increased; however, after 6D, the power coefficient value reduce as the distance increased.

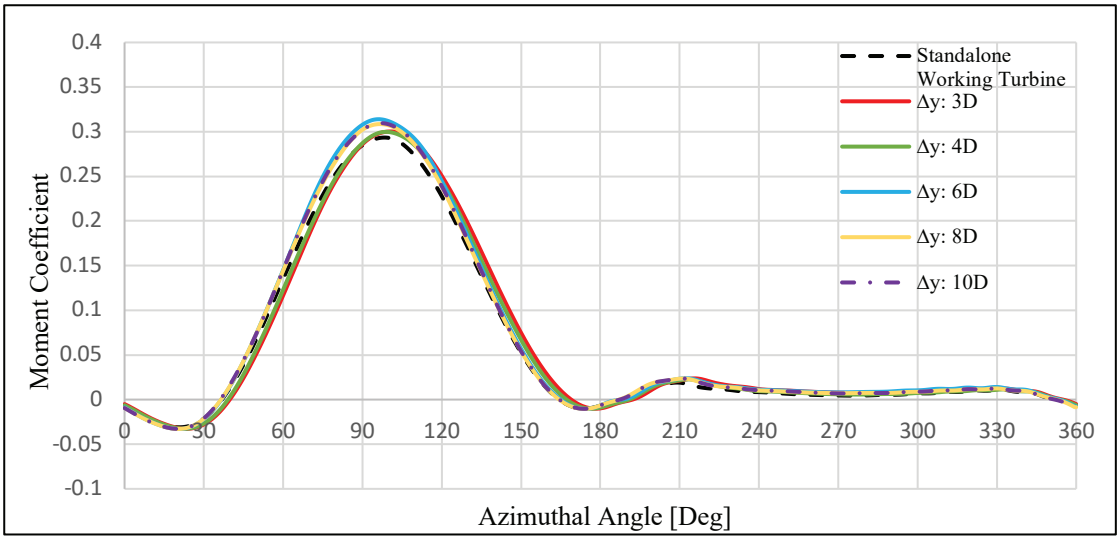

Figure 3.13 Instantaneous one-blade Cp for the Vertical Axis Wind Turbines working in pairs, compared to the isolated turbine at TSR 2.2

While there was a considerable difference in power coefficient values compared to a standalone turbine, the relationship between distance and power coefficient values became less significant as the distance increased, particularly after 6D. The power coefficient output between 6D and 8D distances differed by only 2%, while the difference between 10D and 8D distances was 1.2%. These differences are within the margin of error, indicating that the increase in the distance beyond 6D does not have a significant impact on the power coefficient. Nevertheless, the turbines working in pairs still exhibited an approximately 10% improvement in performance compared to the standalone working turbine at TSR 2.2.

Figure 3.14 shows that the instantaneous moment coefficient values of VAWTs operating at TSR 3.3 and placed at 3D, 4D, 6D, 8D, and 10D distances from each other. At TSR 3.3, the maximum power coefficient value was observed at a distance of 3D between the turbines, which shows an important improvement of %46.42 over the standalone turbine, in contrast to the CFD simulation results at TSR 1.7. The improvement in power coefficient decreased as the space between the turbines increased, becoming insignificant beyond 8D. The difference in power coefficient values between turbines working in pairs at distances of 4D, 6D, 8D, and 10D and the standalone turbine were %34.8, %24, %11.5, and %8.2, respectively.

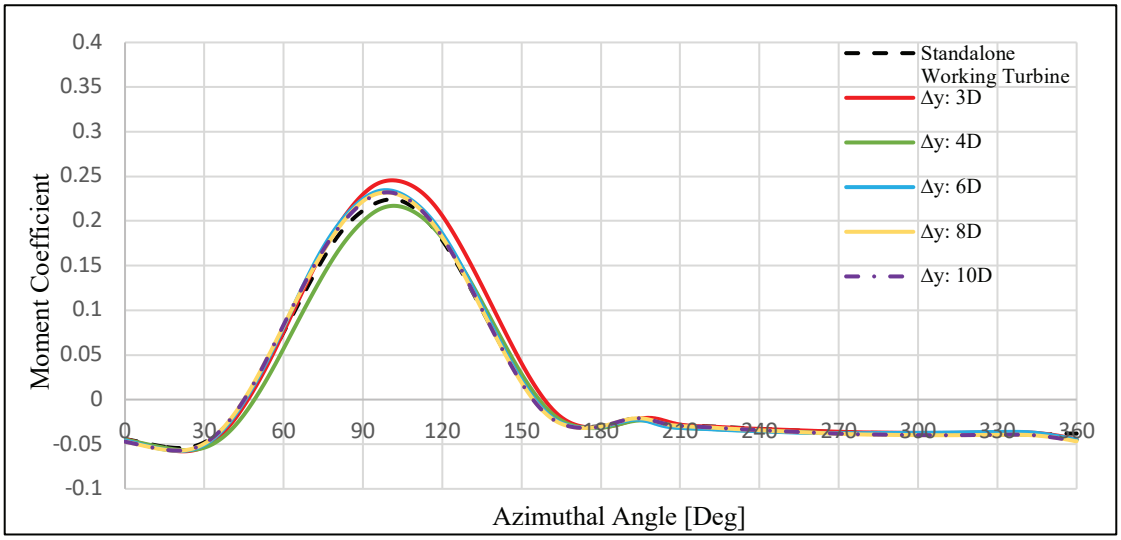

Figure 3.14 Instantaneous one-blade Cp for the Vertical Axis Wind Turbines working in pairs, compared to the isolated turbine at TSR 3.3

Ultimately, the moment coefficient values obtained from a full rotation of the turbines operating at TSR 4.4 are shown in Figure 3.15. As seen in the figure, the turbines located at varying distances displayed identical characteristics for both working in pairs and standalone working turbines. The results of CFD simulations performed at TSR 4.4 showed that the turbines produced a negative power coefficient output.

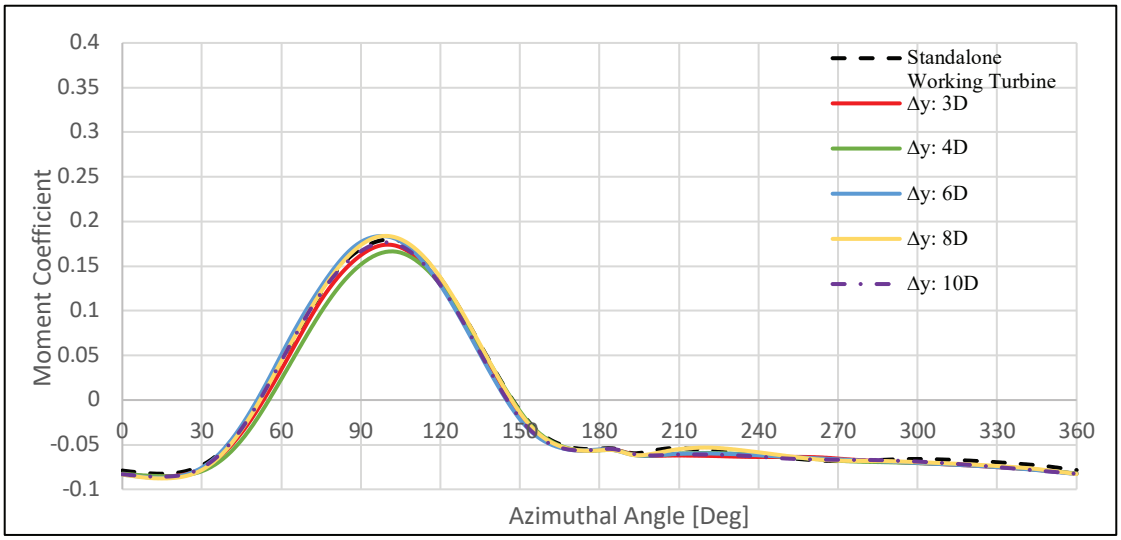

Figure 3.15 Instantaneous one-blade Cp for the Vertical Axis Wind Turbines working in pairs, compared to the isolated turbine at TSR 4.4

The standalone working turbine and the turbines working in pairs located at a 3D distance produced a similar negative power coefficient. The remarkable finding from these simulations was that the absolute value of the negative power coefficient increased with the increase in the distance between the turbines. Unlike the results obtained from other TSRs, the effect of distance on the turbines remained significant even after 6D distance. In TSR 4.4, the largest distance of 10 between the turbines still had an impact on the power coefficient.

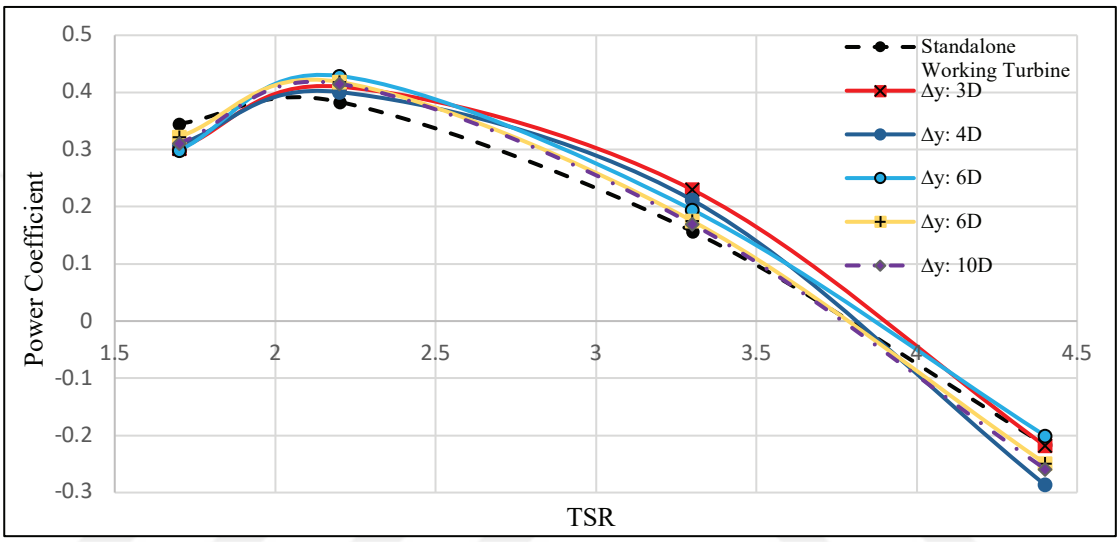

Figure 3.16 Cp Vs TSR

In figure 3.16, the results from the CFD simulations made at various TSRs (TSR 1.7, TSR 2.2, TSR 3.3, TSR 4.4) for the study of standalone working turbines and turbines that work in pairs located at various distances (3D, 4D, 6D, 8D, 10D) to each other are presented in a single graph. The results show that the highest performance gain of %46.42 was achieved from the turbines located with a 3D distance at TSR 3.3.

However, in TSR 1.7, the performance of the turbines that worked in pairs negatively impacted each other, resulting in a %12.61 decrease on the power coefficient compared to the standalone turbine. As the distance between the turbines increased, this negative effect on the turbines decreased. At TSR 2.2, although the turbines located at 3D distances showed a %6.93 increase in performance compared to the standalone working turbine, and the effect of the distance on the performance of turbines increased up to 6D, these values remained below the margin of error, making the effect of distance in between the two turbines on performance in TSR 2.2 insignificant.

The TSR 3.3 was the most optimal operating speed for observing the impact of the distance of the turbines on their performance. The performance improvement of the turbines that were working in pairs compared to the standalone turbine decreased as the distance between the two turbines increased, and this decrease was clearly visible up to 8D. At TSR 4.4, the turbines that were located at a 3D distance behaved similarly to a standalone turbine with only a %0.84 difference in power coefficient. However, as the distance between the two turbines increased, the negative power coefficient value also increased. The effect of the distance between the turbines on their performance was significant at all distances studied in the CFD simulation.

Figure 3.17 shows the power coefficient values obtained by Zanforlin et al. (*18*) from different TSRs of two turbines with a 1.5D distance from each other, compared to a single standalone turbine. The results of the CFD simulations of the present study are compared with those obtained by Zanforlin et al. (*18*). Although the parameters of the CFD simulations, the geometry of the fluid domain, the geometry of the turbines, and the direction of rotation of the turbines in the present study are not identical to those of Zanforlin et al. (*18*), but the results are still comparable. Zanforlin et al. achieved a % 40 performance gain with turbines that working in pairs with 1.5D distance between each other's at TSR 3.1 and an % 8 performance gain at 2.3 TSR with the same simulation domain geometry.

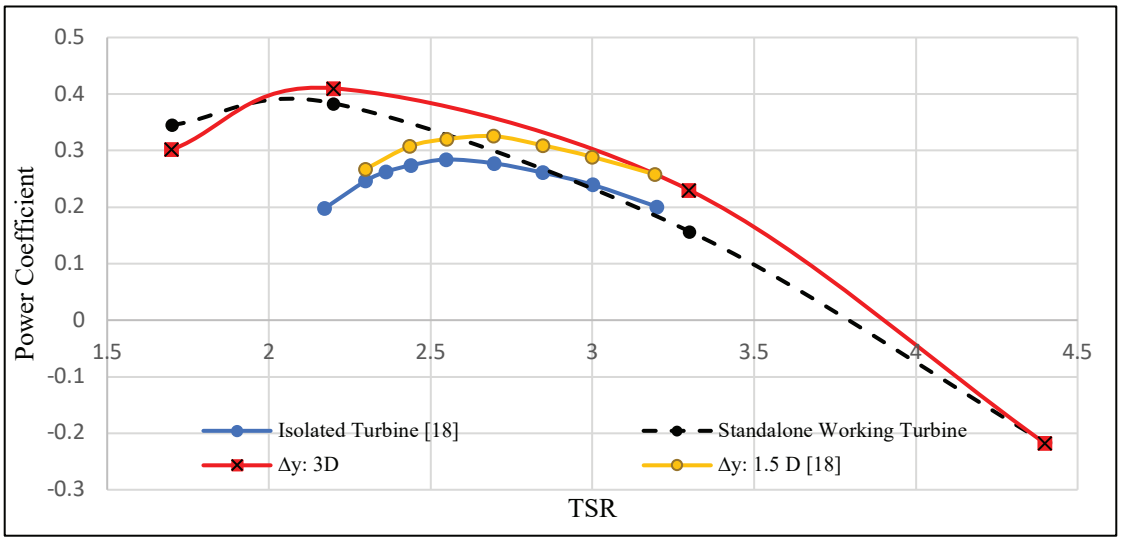

Figure 3.17 Comparison of power coefficient vs TSR

The current study's results show a performance increase of % 6.3 at TSR 2.2 and % 46 at TSR 3.3 with the turbines working in pairs with 3D distance between each other's, which are nearly similar to the results obtained by Zanforlin et al (*18*).

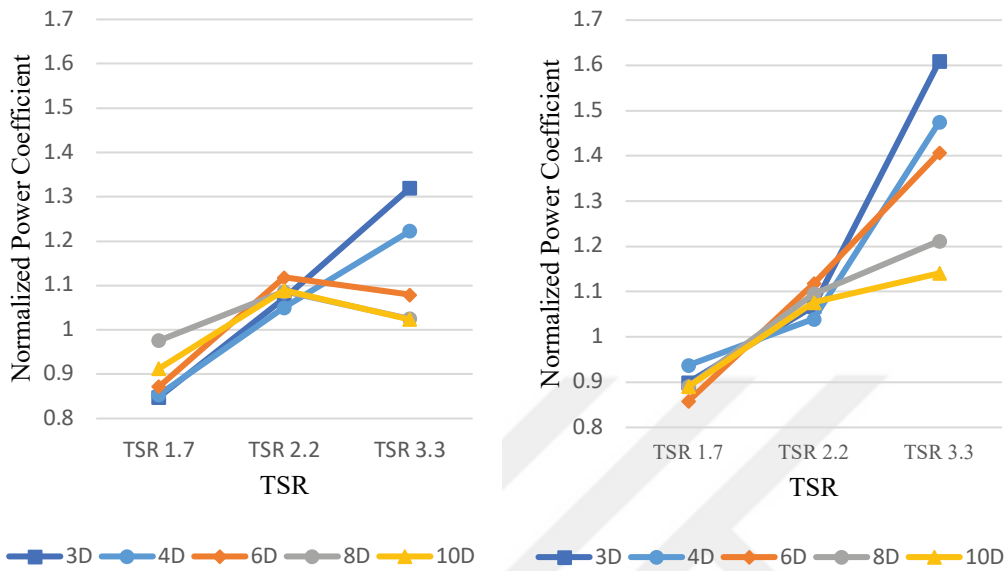

Figure 3.18 Normalized power coefficient values of Turbine-1 (Left) and Turbine-2 (Right) at various TSR's

Figure 3.18 illustrates the normalized power coefficient values of a pair of VAWT turbines in different tip-speed ratios (TSRs) and distances. The results indicate that Turbine-2 outperformed Turbine-1 in terms of power coefficient. Turbine-1 demonstrated its best performance at TSR 2.2 for distances of 6D, 8D, and 10D. However, the increase in TSR for Turbine-2 resulted in a higher performance gain, and the rate of increase in performance decreases as the distance between the turbines increased.

Based on Figure 3.19, a comparison was made between the normalized power coefficient values of Turbine-1, Turbine-2, and the average of these two turbines, against the normalized power coefficient values obtained by Zanforlin et al. (*18*) for various TSRs. The graph indicates that the normalized power coefficient of Turbine-1 closely matches the values obtained by Zanforlin et al. (*18*).

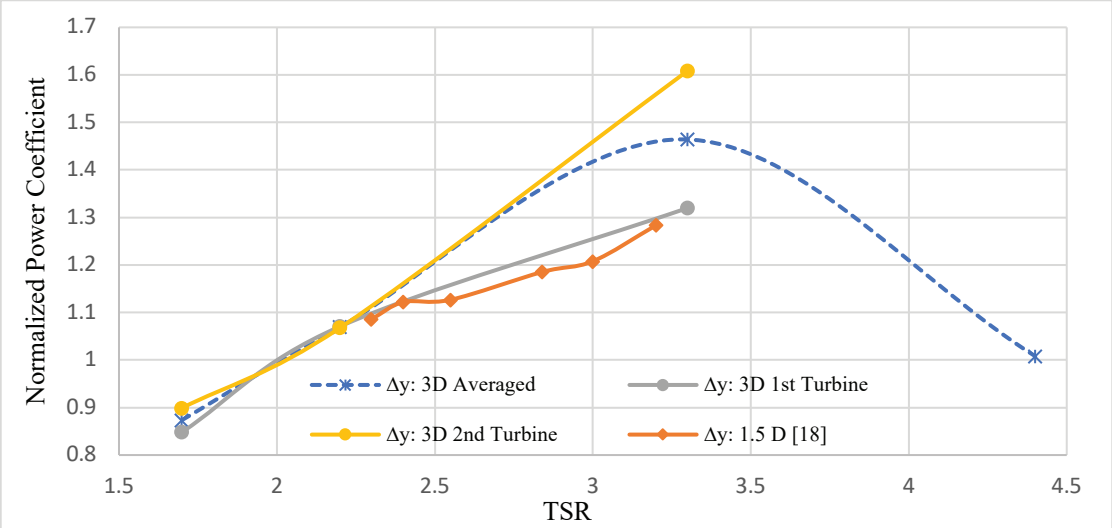

Figure 3.19 Comparison of normalized power coefficient vs TSR

CHAPTER 4

CONCLUSION

This thesis investigated the impact of inter-turbine distance on the performance of VAWTs at various TSRs. To examine the performance improvement achieved by turbine pairs located at different distances, standalone VAWTs with the same turbine and blade design were used as a basis for comparison. In order to ensure accurate and reliable results, one-bladed standalone VAWT was validated using published reference studies, and the moment coefficient values obtained from one-bladed standalone VAWT at various TSRs were compared to these reference studies. Mesh independency analysis and time step sensitivity analysis studies were conducted to determine the optimal simulation settings and parameters for the CFD simulations.

After the one-bladed VAWT simulation results were validated against the reference study, performance comparisons were made between one-bladed, two-bladed, and three-bladed standalone VAWTs to reveal the effect of the inter-turbine blade interaction on the energy output. It was found that increasing the number of blades in a standalone VAWT resulted in a reduction in performance due to increased solidity. This effect was not clearly observed at low TSRs, such as TSR 1.7, due to flow separation caused by the angle of attack and vortex formed on the airfoil boundary layer. Therefore, VAWTs are unstable at low TSRs. As TSR increased, the vortex disappeared with a decrease in the angle of attack, resulting in improved performance in the one-bladed VAWTs at high TSRs. However, increasing the number of blades reduced the performance of the VAWT operating at high TSR due to the wake flow of each blade. Each new blade created a new wake flow for the blade behind it, and as the rotational speed of the turbine increased, the interaction of the blades with the wake flow of the front blade increased, resulting in reduced VAWT performance. Finally, the results showed that the one-bladed VAWT performed best at TSR 3.3, while the two-bladed and three-bladed VAWTs performed best at TSR 2.2.

In the second part of Chapter 3, the effect of inter-turbine distance and various TSRs on performance was investigated using co-rotating turbines located at various distances and operating at various TSRs. When VAWTs operate together at low TSRs, where the angle of attack is high, the negative effect of the pressure zone between the two

turbines can cause a reduction in the performance of VAWTs due to the changes in the drag/lift force ratio. However, as the distance between the two turbines increases, this pressure zone loses its negative effect, and the reduction in performance becomes less significant. However, Since the turbines work stably at high TSRs, this effect improves the performance of the VAWT.

The results of the study show that, contrary to findings in previous literature, there was a decrease in the of performance VAWTs at TSR 1.7. Despite the fact that the reduction in performance decreases as the distance between turbines increases, even at a distance of 10D between turbines, a 10% decrease in power coefficient was still observed. In contrast, for turbines operating at TSR 2.2 and located at different distances, a % 6.9 performance improvement was achieved compared to a standalone working turbine at a distance of 3D, and this performance increase persisted up to a distance of 6D. Although the performance gain decreased from 6D to 10D, the observed reduction in performance was considered to be insignificant. The performance improvements observed at TSR 2.2 were consistent with those reported in De Tavernier et al.'s (*21*) study. The study found that at TSR 3.3 and with a 3D distance between turbines, there was a % 46 increase in performance compared to a standalone working turbine. While such a significant increase has not been reported in any previous studies, it is noteworthy that the NACA0018 profile blade was found to work most efficiently at TSR 3.5 (*19*). Despite the decrease in performance gain as the distance between turbines increases at TSR 3.3, there was still an % 8 performance increase at a distance of 10D between the turbines.

Lastly, the study found that turbines with a 3D distance between them at TSR 4.4 exhibited the same performance as the standalone working turbine. Even when the turbines were placed at a distance of 6D from each other and produced negative power, they still performed % 7.3 better than the standalone working turbine.

In future studies, there is potential to investigate the distance between turbines and the Tip Speed Ratio with greater precision. Prior CFD simulations have adjusted the angular velocity of the turbine to change the TSR while holding the freestream velocity constant at 8m/s. By maintaining a constant TSR, researchers can evaluate the effect of turbine permeability on performance by modifying both the freestream velocity and the angular velocity of the turbine.

CHAPTER 5

REFERENCES

(1) Kumar, P. M.; Sivalingam, K.; Narasimalu, S.; Lim, T.-C.; Ramakrishna, S.; Wei, H. A Review on the Evolution of Darrieus Vertical Axis Wind Turbine: Small Wind Turbines. J.Power Energy Eng. 2019, 07 (04), 27–44. https://doi.org/10.4236/jpee.2019.74002.

(2) Hall, T. J. Numerical Simulation of a Cross Flow Marine Hydrokinetic Turbine.

(3) Yang, Y.; Guo, Z.; Zhang, Y.; Jinyama, H.; Li, Q. Numerical Investigation of the Tip Vortex of a Straight-Bladed Vertical Axis Wind Turbine with Double-Blades. Energies 2017, 10 (11), 1721. https://doi.org/10.3390/en10111721.

(4) Wilcox, D. Turbulence Modeling for CFD (Third Edition); 2006.

(5) Celik, I. B. Introductory Turbulence Modeling.

(6) Strickland, J. H.; Webster, B. T.; Nguyen, T. A Vortex Model of the Darrieus Turbine: An Analytical and Experimental Study. J. Fluids Eng. 1979, 101 (4), 500–505. https://doi.org/10.1115/1.3449018.

(7) Vittecoq, P.; Laneville, A. The Aerodynamic Forces for a Darrieus Rotor with Straight Blades: Wind Tunnel Measurements. J. Wind Eng. Ind. Aerodyn. 1983, 15 (1), 381–388. https://doi.org/10.1016/0167-6105(83)90207-6.

(8) Kooiman, S.; Tullis, S. Response of a Vertical Axis Wind Turbine to Time Varyin Wind Conditions Found within the Urban Environment. Wind Eng. 2010, 34. https://doi.org/10.1260/0309-524X.34.4.389.

(9) Castelli, M. R.; Garbo, F.; Benini, E. Numerical Investigation of Laminar to Turbulent Boundary Layer Transition on a Naca 0012 Airfoil for Vertical-Axis

Wind Turbine Applications. Wind Eng. 2011, 35 (6), 661–685. https://doi.org/10.1260/0309-524X.35.6.661.

(10) Sheldahl, R. E.; Klimas, P. C. Aerodynamic Characteristics of Seven Symmetrical Airfoil Sections through 180-Degree Angle of Attack for Use in Aerodynamic Analysis of Vertical Axis Wind Turbines; United States, 1981. https://doi.org/10.2172/6548367.

(11) Balduzzi, F.; Bianchini, A.; Ferrara, G.; Ferrari, L. Dimensionless Numbers for the Assessment of Mesh and Timestep Requirements in CFD Simulations of Darrieus Wind Turbines. Energy 2016, 97, 246–261. https://doi.org/10.1016/j.energy.2015.12.111.

(12) Rezaeiha, A.; Kalkman, I.; Blocken, B. CFD Simulation of a Vertical Axis Wind Turbine Operating at a Moderate Tip Speed Ratio: Guidelines for Minimum Domain Size and Azimuthal Increment. Renew. Energy 2017, 107, 373–385. https://doi.org/10.1016/j.renene.2017.02.006.

(13) Whittlesey, R. W.; Liska, S.; Dabiri, J. O. Fish Schooling as a Basis for Vertical Axis Wind Turbine Farm Design*. Bioinspir. Biomim. 2010, 5 (3), 035005. https://doi.org/10.1088/1748-3182/5/3/035005.

(14) Schatzle, P. R.; Klimas, P. C.; Spahr, H. R. Aerodynamic Interference Between Two Darrieus Wind Turbines. J. Energy 1981, 5 (2), 84–88. https://doi.org/10.2514/3.62505.

(15) Dabiri, J. O. Potential Order-of-Magnitude Enhancement of Wind Farm Power Density via Counter-Rotating Vertical-Axis Wind Turbine Arrays. J. Renew. Sustain. Energy 2010, 3, 043104.

(16) Brownstein, I.; Wei, N.; Dabiri, J. Aerodynamically Interacting Vertical-Axis Wind Turbines: Performance Enhancement and Three-Dimensional Flow. Energies 2019, 12, 2724. https://doi.org/10.3390/en12142724.

(17) Kinzel, M.; Mulligan, Q.; Dabiri, J. O. Energy Exchange in an Array of Vertical-Axis Wind Turbines. J. Turbul. 2012, 13, N38. https://doi.org/10.1080/14685248.2012.712698.

(18) Zanforlin, S.; Nishino, T. Fluid Dynamic Mechanisms of Enhanced Power Generation by Closely Spaced Vertical Axis Wind Turbines. Renew. Energy 2016, 99, 1213–1226. https://doi.org/10.1016/j.renene.2016.08.015.

(19) Brusca, S.; Lanzafame, R.; Messina, M. Design of a Vertical-Axis Wind Turbine: How the Aspect Ratio Affects the Turbine's Performance. Int. J. Energy Environ. Eng. 2014, 5 (4), 333–340. https://doi.org/10.1007/s40095-014-0129-x.

(20) Guilbot, M.; Barre, S.; Balarac, G.; Bonamy, C.; Guillaud, N. A Numerical Study of Vertical Axis Wind Turbine Performances in Twin-Rotor Configurations. J. Phys. Conf. Ser. 2020, 1618, 052012. https://doi.org/10.1088/1742-6596/1618/5/052012.

(21) De Tavernier, D.; Ferreira, C.; Li, A.; Paulsen, U. S.; Madsen, H. A. Towards the Understanding of Vertical-Axis Wind Turbines in Double-Rotor Configuration. J. Phys. Conf. Ser. 2018, 1037, 022015. https://doi.org/10.1088/1742-6596/1037/2/022015.

(22) Model Evaluation Guidance and Protocol Document: COST Action 732 Quality Assurance and Improvement of Microscale Meteorological Models; Britter, R., Baklanov, A., Eds.; Univ. of Hamburg, Meteorological Inst: Hamburg, 2007.

(23) G. J. M. Darrieus, Turbine having its rotational shaft traverse to the flow of the current (1931)

(24) J. Hoffman and C. Johnson, Computational turbulent incompressible flow: Applied mathematics: Body and soul 4, vol. 4. 2007. doi: 10.1007/978-3-540-46533-1.

(25) T. Ahmad, S. L. Plee, and J. P. Myers, "Ansys Fluent Theory Guide".

(26) Grzegorz. Łukaszewicz, Navier–Stokes Equations An Introduction with Applications, 1st ed. 2016. 2016.

(27) Hand, B.; Cashman, A. A Review on the Historical Development of the Lift-Type Vertical Axis Wind Turbine: From Onshore to Offshore Floating Application. *Sustain. Energy Technol. Assess.* 2020, *38*, 100646. https://doi.org/10.1016/j.seta.2020.100646.

(28) Manwell, J.; Mcgowan, J.; Rogers, A. Wind Energy Explained: Theory, Design and Application, Second Edition. In *Wind Engineering*; 2006; Vol. 30. https://doi.org/10.1260/030952406778055054.